Revisiting Outage Probability Analysis for Two-User Fluid Antenna Multiple Access System

Hao Xu, *Member, IEEE*, Kai-Kit Wong, *Fellow, IEEE*, Wee Kiat New, *Member, IEEE*, Kin-Fai Tong, *Fellow, IEEE*, Yangyang Zhang, and Chan-Byoung Chae, *Fellow, IEEE*

***Abstract*—Fluid antenna system (FAS) is a new flexible antenna technology that offers a new approach to multiple access, referred to as fluid antenna multiple access (FAMA). The performance of FAMA has been investigated but previous results were based on simplified spatial correlation models. In this paper, we will revisit FAMA for the two-user case and study the outage probability by characterizing the joint spatial correlation among the ports. We first derive a closed-form lower bound on the outage probability and reveal that in the absence of spatial correlation, the outage probability of the system decreases exponentially as the number of ports increases. We then show that the channel model can be greatly simplified by focusing upon a limited number of channel variables, allowing us to derive the outage probability using the approximate model. To gain insight, we further approximate the channel model and provide another approximation of the outage probability that is easier to compute. Simulation results validate the approximations and demonstrate that the outage probability decreases with the number of ports but has an error floor unless the antenna size is increased. Also, when the number of ports is fixed, the outage probability initially decreases exponentially with the size but eventually approaches the lower bound.**

***Index Terms*—Fluid antenna, fluid antenna multiple access, outage probability, spatial correlation.**

I. Introduction

Due to the limited radio spectrum and the explosive growth of mobile data and devices, massive connectivity has become a major driver for the fifth generation (5G) and beyond mobile communication systems [1]. Realizing massive connectivity is however a difficult task. Massive multiple-input multiple-output (MIMO) [2], [3] is currently the *de facto* technology in 5G to support a large number of users on the same channel by separating multiuser signals in the spatial domain while non-orthogonal multiple access (NOMA) [4], [5], [6] is an ambitious scheme to overload the spectrum by requiring each user with intelligent power allocation to eliminate inter-user interference utilizing interference cancellation. Under practical conditions, both techniques however could struggle to cope. One reason is that channel state information (CSI) is required at the base station (BS) and complex optimization (precoding for massive MIMO and user clustering and power control for NOMA) needs to be performed, limiting their scalability. In 5G, massive MIMO is not designed to serve more than 12 users while NOMA (or rate-splitting multiple access (RSMA) [7]) is too expensive to handle more than 3 users.

To improve scalability, we need a much simpler approach, one that scales better with the number of users and requires less CSI at the BS. To this end, recent efforts in fluid antenna system (FAS) show potential [8], [9]. Specifically, if a user is equipped with FAS, the user will have the ability to scan through the channels in the spatial domain and choose to receive the signal at the position (referred to as 'port') where the interference suffers from a deep fade. This is referred to as fluid antenna multiple access (FAMA). FAS relies on flexible antenna technologies that may come in the form of liquid-based antennas [10], [11], [12], reconfigurable RF pixel-based antennas [13], [14], [15], stepper motor-based antennas [16], [17], and flexible structures using metamaterials [18].

Despite being a new topic, recent researches in FAS already cover single-user [19], [20], [21], [22], [23], [24], [25] and multiuser systems [26], [27], [28]. The interest of this paper will be on the multiuser scenario where FAS is used primarily for multiple access. FAMA was first introduced in 2022 by Wong and Tong [26]. The idea of FAMA lies in the fact that multiuser signals fade independently in space and as such, the FAS at a given user can find and operate at the port where the interfering users all fade deeply to have interference-less signal reception for communication. Depending on how fast the user updates the port of FAS, FAMA can be classified into fast [26], [27] and slow FAMA [28].

Fast FAMA requires each user to switch its port on a symbol-by-symbol basis while slow FAMA is more practical and only has users switching their ports if their channels change. In [28], it was demonstrated that several users can be accommodated on the same channel using slow FAMA to achieve a high multiplexing gain without CSI at the BS side and interference cancellation receivers at the users. In [29], an analytical framework for the outage performance of large-scale FAS-enabled communications was presented, where all users employ a circular multi-FAS array. To reduce the channel estimation overhead, a novel sequential linear minimum mean-

The work of H. Xu, K. Wong, W. K. New, and K. Tong is supported in part by the European Union's Horizon 2020 Research and Innovation Programme under MSCA Grant No. 101024636, and in part by the Engineering and Physical Sciences Research Council (EPSRC) under grant EP/W026813/1. The work of C. B. Chae is supported by the Institute for Information and Communication Technology Promotion (IITP) grant funded by the Ministry of Science and ICT (MSIT), Korea (No. 2021-0-02208, No. 2021-0-00486, 2022R1A5A1027646).

Part of this work has been presented in IEEE International Conference on Communication (ICC) 2023 [33].

H. Xu, K. Wong, W. K. New and K. Tong are with the Department of Electronic and Electrical Engineering, University College London, London WC1E7JE, United Kingdom. K. Wong is also affiliated with Yonsei Frontier Laboratory, Yonsei University, Seoul, 03722, Korea (e-mail: {hao.xu, kai-kit.wong, a.new, k.tong}@ucl.ac.uk).

Y. Zhang is with Kuang-Chi Science Limited, Hong Kong SAR, China (e-mail: yangyang.zhang@kuang-chi.org).

C. B. Chae is with School of Integrated Technology, Yonsei University, Seoul, 03722, Korea (e-mail: cbchae@yonsei.ac.kr).

Corresponding author: Kai-Kit Wong (e-mail: kai-kit.wong@ucl.ac.uk).

TABLE I
LIST OF NOTATIONS

Notation	Definition	Notation	Definition
$W\lambda$	Size of the fluid antenna, where W is the normalized size and λ is the wavelength	M, L	Key parameters in the approximation
N	Number of ports	$p_{\text{out},k}(r_k)$	Outage probability of the FAMA system
s_j	Data symbol intended for user j	$\tilde{g}_{j,k}^{(n)}, \hat{g}_{j,k}^{(n)}, \hat{g}_{j,k}^{n,l}, \overline{g}_{j,k}^{n,l}$	Approximations of $g_{j,k}^{(n)}$
$g_{j,k}^{(n)}$	Channel gain from the j-th BS antenna to the n-th port of user k	$\Phi_k^{(n)}$	$\Phi_k^{(n)} = \lvert\hat{g}_{k,k}^{(n)}\rvert/\lvert\hat{g}_{\bar{k},k}^{(n)}\rvert$
$\eta_k^{(n)}$	Additive Gaussian noise	$\hat{\Phi}_k^{n,l}$	$\hat{\Phi}_k^{n,l} = \lvert\hat{g}_{k,k}^{n,l}\rvert/\lvert\hat{g}_{\bar{k},k}^{n,l}\rvert$
$y_k^{(n)}$	Received signal at the n-th port of user k	$\hat{\Psi}_k$	$\hat{\Psi}_k = \max\left\{\hat{\Phi}_k^{n,l}, 1 \le n \le N, 1 \le l \le L\right\}$
$\boldsymbol{g}_{j,k}$	$(g_{j,k}^{(1)}, \ldots, g_{j,k}^{(N)})^T$	$\overline{\Phi}_k^{n,l}$	$\overline{\Phi}_k^{n,l} = \lvert\overline{g}_{k,k}^{n,l}\rvert/\lvert\overline{g}_{\bar{k},k}^{n,l}\rvert$
$\sigma_{j,k}^2\boldsymbol{\Sigma}$	Covariance matrix of $\boldsymbol{g}_{j,k}$	$\overline{\Psi}_k$	$\overline{\Psi}_k = \max\left\{\overline{\Phi}_k^{n,l}, 1 \le n \le N, 1 \le l \le L\right\}$
$\boldsymbol{U\Theta U}^H$	Eigenvalue decomposition of $\boldsymbol{\Sigma}$	$J_0(\cdot)$	Zero-order Bessel function of the first kind
γ_{th}	SIR threshold	$Q_1(\cdot,\cdot)$	Marcum Q-function of order 1
r_k	$r_k = \sqrt{\gamma_{\text{th}} p_{\bar{k}}/p_k}$	$I_0(\cdot)$	Modified Bessel function of the first kind

squared error (LMMSE)-based channel estimation method was performed for only a very small number of antenna ports. It was shown that the developed framework can accurately capture the channel estimation errors on the performance of the considered network deployments. In [30], the NOMA and FAS techniques are combined to expand the communication range of a downlink millimeter wave (mmWave) system.

Accurate performance evaluation is crucial in understanding the true potential of FAMA but the performance analysis of FAMA so far has been limited to a simplified channel model [31], which is unable to accurately characterize the spatial correlation amongst the ports of the FAS. In [32], Khammassi *et al.* adopted the eigenvalue-based model to fully account for the channel correlation over the ports, and revealed that the outage probability performance for a single-user FAS could be quite different from what was originally reported in [19]. In particular, the results in [32] illustrated that increasing the number of ports (i.e., the spatial resolution of FAS) has a diminishing return. However, the situation in FAMA is much less understood. In [33], the eigenvalue-based channel model was considered for a two-user slow FAMA system.

In this paper, we extend the work of [33] focusing on the two-user slow FAMA system.[1] Our goal is to approximate the fully correlated channel model, analyze the outage probability of the system based on the accurate but simplified model, and gain more insights on how the performance scales with the fluid antenna size W and the number of ports N. The main contributions of this work are summarized below.

- Assuming that each user has access to the received signals from all ports, we first derive a closed-form lower bound on the outage probability. We show that this bound can be viewed as the outage probability of a special FAMA system with no spatial correlation among the ports. In this idealized scenario, increasing N provides each user with a larger number of alternatives in selecting a port with minimal interference. Consequently, the lower bound experiences an exponential reduction with an increase in N and can thus be arbitrarily small. As we will analyze and also show by simulations, this is quite different from the real FAMA system since the channel gains of different ports are usually highly correlated.
- Although the eigenvalue-based channel model in [32] can accurately characterize the spatial correlation among the ports, it results in expressions involving N nested integrals in the analysis of the outage probability, which are computationally intractable. To facilitate the analysis, we show that the channel model is determined by a Hermitian Toeplitz matrix whose energy is mainly concentrated in a few largest eigenvalues. As a result, it is possible to approximate each channel coefficient by considering M dominant eigenvalues, where M is considerably smaller than N. Based on this simplified channel model, the outage probability of the system is analyzed. However, despite the significant simplification achieved in the first stage, the approximated outage probability is still difficult to compute, as it is a $4M$-fold integral. Therefore, we extend the second-stage approximation scheme for the single-user FAS in [32] to the FAMA system. Adopting this new model, another approximation of the outage probability is derived and expressed as a 2-fold integral, which is easy to compute and more insightful.
- Simulation results validate the performance of the two-stage scheme in approximating the channel model. We see that as N increases while the normalized size of the fluid antenna W is fixed, the outage probability initially decreases dramatically. However, it eventually saturates due to the strong inter-correlation between closely spaced ports, which suggests that an excessive increase in N does not lead to additional gain if W is fixed. Furthermore, for a given N, we observe that the outage probability decreases almost exponentially as W increases at the beginning and then approaches the lower bound we have derived. This indicates that increasing the size of a fluid

[1]This paper improves [33] by further simplifying the analysis and making the resulting expressions more tractable. In contrast to [33], the distinctive contributions of this paper include: a closed-form lower bound on the outage probability that serves as a benchmark; a second-stage approximation of the channel model and the outage probability analysis based on it; and more insightful observations derived from both the analysis and simulation results.

This article has been accepted for publication in IEEE Transactions on Wireless Communications. This is the author's version which has not been fully edited and content may change prior to final publication. Citation information: DOI 10.1109/TWC.2024.3363499

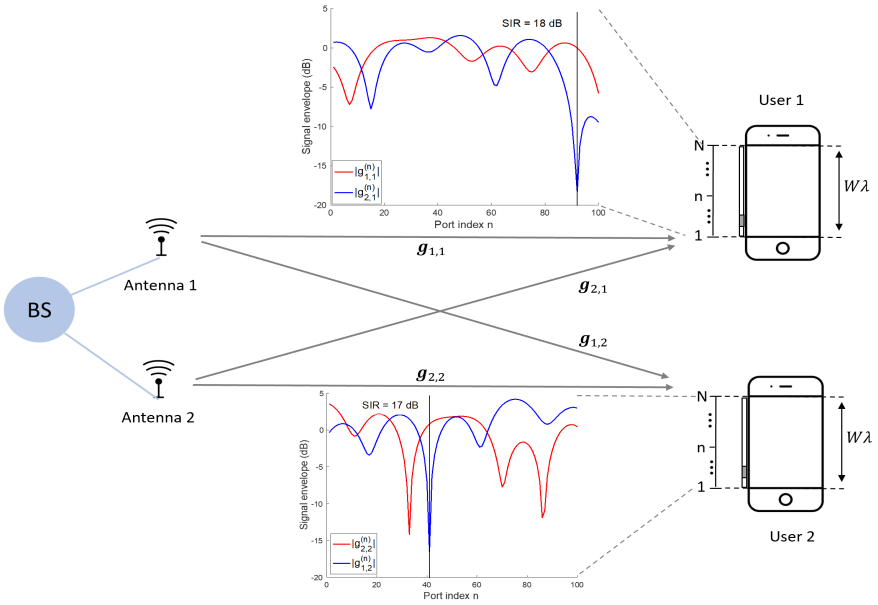

Fig. 1. A downlink slow FAMA system with a BS using two fixed antennas to communicate to two FAS-assisted users.

antenna can significantly improve the performance of the FAMA system, especially when W is small.

The remainder of this paper is organized as follows. In Section II, we introduce the two-user FAMA system and the exact channel model. Section III provides the analysis of outage probability. Section IV then attempts to make some interesting observations of two-user FAMA using some numerical results. Finally, Section V draws some concluding remarks. Auxiliary technical results are given in the appendices.

Notations: We use boldface upper and lower case letters to denote matrices and column vectors. $\mathbb{E}[\cdot]$ and $\mathrm{Cov}[\cdot]$ are respectively the statistical expectation and covariance. $\mathcal{CN}$ represents the complex Gaussian distribution. $(\cdot)^T$ and $|\cdot|$ stand for transpose and magnitude, respectively. $(\cdot)_{n,n'}$ denotes the element of a matrix in the n-th row and n'-th column. To help readers follow the mathematical contents, the meanings of some key notations are summarized in Table I.

II. System Model and Problem Formulation

As shown in Fig. 1, we consider a downlink slow FAMA system, comprising a BS and two users. The BS has two fixed antennas, while each user is equipped with a FAS. Each BS antenna serves one particular user. Without loss of generality, we assume that the k-th antenna at the BS serves user k. The fluid antenna's location can be instantaneously switched to one of the N predetermined ports, which are evenly distributed along a linear dimension of length $W\lambda$ and share a common radio frequency (RF) chain.[2] Then, the received signal at the n-th port of user k is given by

$$y_k^{(n)} = \sum_{j=1}^{2} g_{j,k}^{(n)} s_j + \eta_k^{(n)}, \text{ for } k = 1, 2, \tag{1}$$

[2]This structure can be seen as an approximation of an RF pixel-based linear FAS that has many compact antenna pixels, among which one antenna (formed by several pixels) can be activated at each time [34]. Using this technology, it is possible to switch the antennas with almost no time delay.

where $s_j \sim \mathcal{CN}(0, p_j)$ denotes the signal intended for user j, $g_{j,k}^{(n)} \sim \mathcal{CN}(0, \sigma_{j,k}^2)$ is the channel coefficient from the j-th BS antenna to the n-th port of user k, and $\eta_k^{(n)} \sim \mathcal{CN}(0, \sigma_0^2)$ denotes the additive white Gaussian noise. Here p_j and σ_0^2 are respectively the signal and noise power, and $\sigma_{j,k}^2$ can be seen as the large-scale fading of the link from the j-th BS antenna to user k.

Let $\boldsymbol{g}_{j,k} = \left(g_{j,k}^{(1)}, \ldots, g_{j,k}^{(N)}\right)^T$ and $\boldsymbol{\Sigma}_{j,k} = \sigma_{j,k}^2 \boldsymbol{\Sigma}$ be the covariance matrix of $\boldsymbol{g}_{j,k}$. As in [19] and [26], the spatial correlation over the ports is characterized based on the Jake's model [35]. Thus, the (n, n')-th entry of $\boldsymbol{\Sigma}$ is given by

$$\begin{aligned}(\boldsymbol{\Sigma})_{n,n'} &= \frac{1}{\sigma_{j,k}^2} \mathrm{Cov}\left[g_{j,k}^{(n)}, g_{j,k}^{(n')}\right] \\ &= J_0\left(\frac{2\pi|n-n'|\lambda\Delta}{\lambda}\right) \\ &= J_0\left(2\pi(n-n')\Delta\right), \end{aligned} \tag{2}$$

where $\Delta = W/(N-1)$ is the normalized distance between any two adjacent ports and $J_0(\cdot)$ is defined in Table I.

Considering that a FAS usually has a large number of ports, it would be very complicated and time-consuming to estimate the full CSI, i.e., $\boldsymbol{g}_{j,k}, \forall j, k \in \{1, 2\}$, if all the ports are involved in the estimation. There have been some works studying the performance of FAS-assisted systems with channel estimation errors and the channel estimation problem in FAS-assisted systems. For example, in [29], a novel sequential LMMSE-based method was performed to estimate the channel gains for only a very small number of antenna ports. Then, an analytical framework for the outage performance that accurately captures the channel estimation errors was presented. In [36], it was shown that in the case of finite scattering channels, it is possible to transmit a small number of pilots and estimate the sparse channel parameters at only a few selected ports. Then, the full CSI can be reconstructed based

on the geometric channel model. In this paper, we assume that the full CSI is known at the BS for convenience. If only partial CSI is known, one may modify the analysis in this paper by using the technique proposed in [29].

It is known from (1) that the signal-to-interference plus noise ratio (SINR) of user k at the n-th port is found as

$$\gamma_k^{(n)} = \frac{p_k|g_{k,k}^{(n)}|^2}{p_{\bar{k}}|g_{\bar{k},k}^{(n)}|^2+\sigma_0^2} \overset{(a)}{\approx} \frac{p_k|g_{k,k}^{(n)}|^2}{p_{\bar{k}}|g_{\bar{k},k}^{(n)}|^2}, \tag{3}$$

where $\bar{k}=1$ if $k=2$ and $\bar{k}=2$ if $k=1$, and (a) assumes that the interference power is much greater than the noise power. Though SINR provides a more precise measure of the system performance, the signal-to-interference ratio (SIR) serves as a suitable approximation in interference-limited environments.

This paper aims to analyze the outage probability of the considered FAMA system, which is defined as

$$\begin{aligned} p_{\text{out},k}(r_k) &= \Pr\left\{\max\left\{\frac{|g_{k,k}^{(1)}|^2}{|g_{\bar{k},k}^{(1)}|^2},\ldots,\frac{|g_{k,k}^{(N)}|^2}{|g_{\bar{k},k}^{(N)}|^2}\right\} < \frac{\gamma_{\text{th}}p_{\bar{k}}}{p_k}\right\} \\ &= \Pr\left\{\frac{|g_{k,k}^{(1)}|}{|g_{\bar{k},k}^{(1)}|} < r_k,\ldots,\frac{|g_{k,k}^{(N)}|}{|g_{\bar{k},k}^{(N)}|} < r_k\right\}, \end{aligned} \tag{4}$$

where γ_{th} is the SIR threshold and $r_k \triangleq \sqrt{\gamma_{\text{th}}p_{\bar{k}}/p_k}$.

In order to analyze $p_{\text{out},k}(r_k)$ and comprehend the performance of the FAMA system under consideration, it is crucial to model the channel vector $\boldsymbol{g}_{j,k}$ such that it adheres to the aforementioned distribution, i.e., $g_{j,k}^{(n)} \sim \mathcal{CN}(0,\sigma_{j,k}^2)$ and $\mathbb{E}[\boldsymbol{g}_{j,k}\boldsymbol{g}_{j,k}^H] = \sigma_{j,k}^2\boldsymbol{\Sigma}$. As demonstrated in [32], the eigenvalue-based model can effectively achieve this objective by representing each channel coefficient $g_{j,k}^{(n)}$ as a linear combination of N independent and identically distributed (i.i.d.) complex Gaussian random variables. In particular, let $\boldsymbol{U}\boldsymbol{\Theta}\boldsymbol{U}^H$ denote the eigen-decomposition of $\boldsymbol{\Sigma}$, where $\boldsymbol{U}$ is a unitary matrix and $\boldsymbol{\Theta} = \text{diag}\{\theta_1,\ldots,\theta_N\}$ is the eigenvalue matrix, and assume that the eigenvalues in $\boldsymbol{\Theta}$ are arranged in descending order, i.e., $\theta_1 \geq \cdots \geq \theta_N$. Let

$$\boldsymbol{g}_{j,k} = \sigma_{j,k}\boldsymbol{U}\boldsymbol{\Theta}^{\frac{1}{2}}\boldsymbol{x}_{j,k}, \tag{5}$$

where $\boldsymbol{x}_{j,k} = (x_{j,k}^{(1)},\ldots,x_{j,k}^{(N)})^T$ and $x_{j,k}^{(n)} \sim \mathcal{CN}(0,1)$. Note that $x_{j,k}^{(n)}$ can also be expressed as $x_{j,k}^{(n)} = a_{j,k}^{(n)} + ib_{j,k}^{(n)}$, where $a_{j,k}^{(n)}$ and $b_{j,k}^{(n)}$ are i.i.d. real Gaussian variables with zero-mean and variance $\frac{1}{2}$. It can be easily checked that $\boldsymbol{g}_{j,k}$ constructed in (5) satisfies $\mathbb{E}[\boldsymbol{g}_{j,k}\boldsymbol{g}_{j,k}^H] = \sigma_{j,k}^2\boldsymbol{\Sigma}$. In addition, based on (5), the n-th element of $\boldsymbol{g}_{j,k}$, i.e., $g_{j,k}^{(n)}$, can be expressed as

$$\begin{aligned} g_{j,k}^{(n)} &= \sigma_{j,k}\sum_{m=1}^{N}\sqrt{\theta_m}u_{n,m}x_{j,k}^{(m)} \\ &= \sigma_{j,k}\sum_{m=1}^{N}\sqrt{\theta_m}u_{n,m}\left(a_{j,k}^{(m)} + ib_{j,k}^{(m)}\right), \end{aligned} \tag{6}$$

where $u_{n,m}$ is the (n,m)-th element of $\boldsymbol{U}$. Since $J_0(0)=1$, it is known from (2) that $(\boldsymbol{\Sigma})_{n,n}=1$. Then, the variance of $g_{j,k}^{(n)}$ constructed in (6) is given by

$$\sigma_{j,k}^2\sum_{m=1}^{N}\theta_m u_{n,m}^2 = \sigma_{j,k}^2(\boldsymbol{\Sigma})_{n,n} = \sigma_{j,k}^2. \tag{7}$$

Hence, $g_{j,k}^{(n)} \sim \mathcal{CN}(0,\sigma_{j,k}^2)$. The model in (5) and (6) can thus perfectly characterize the distribution of the channel gains and the spatial correlation among the ports. However, using this model for analysis results in expressions involving N nested integrals, which are difficult to compute. Therefore, a channel model that can accurately approximate the strong correlation of fluid antennas, and at the same time, maintain analytical tractability, is of great importance to the study.

III. Main Results

In this section, we analyze the outage probability of the two-user slow FAMA system. We first provide a lower bound on the outage probability. Then as in [32], we approximate the channel model (6) in two steps, and analyze the outage probability of the FAMA system using the simplified models.

A. Lower Bound on the Outage Probability

Let $\boldsymbol{y}_k = (y_k^{(1)},\ldots,y_k^{(N)})^T$ and $\boldsymbol{\eta}_k = (\eta_k^{(1)},\ldots,\eta_k^{(N)})^T$. The received signal of user k, i.e., (1), can be rewritten in a vector form as

$$\boldsymbol{y}_k = \sum_{j=1}^{2}\boldsymbol{g}_{j,k}s_j + \boldsymbol{\eta}_k. \tag{8}$$

Assume that user k can observe the received signals at all ports, i.e., it knows all elements of $\boldsymbol{y}_k$. Obviously, this is an ideal assumption that cannot be realized because each FAS has only one antenna and one RF chain. Therefore, within each symbol, the antenna can only stop at one port and observe the signal at that specific point. We make this assumption here mainly to derive a lower bound on the outage probability in Theorem 1, and we no longer need it in the following subsections. Applying the unitary matrix $\boldsymbol{U}$, resulted from the eigen-decomposition of $\boldsymbol{\Sigma}$, to $\boldsymbol{y}_k$, and using the model of $\boldsymbol{g}_{j,k}$ constructed in (5), we obtain

$$\begin{aligned} \hat{\boldsymbol{y}}_k &= \boldsymbol{U}^H\boldsymbol{y}_k \\ &= \sum_{j=1}^{2}\boldsymbol{h}_{j,k}s_j + \hat{\boldsymbol{\eta}}_k, \text{ for } k=1,2, \end{aligned} \tag{9}$$

where

$$\boldsymbol{h}_{j,k} = \boldsymbol{U}^H\boldsymbol{g}_{j,k} = \sigma_{j,k}\boldsymbol{\Theta}^{\frac{1}{2}}\boldsymbol{x}_{j,k}, \tag{10}$$

and $\hat{\boldsymbol{\eta}}_k = \boldsymbol{U}^H\boldsymbol{\eta}_k \sim \mathcal{CN}(\boldsymbol{0},\sigma_0^2\boldsymbol{I}_N)$. From the definition of $\boldsymbol{x}_{j,k}$ in (5), $\boldsymbol{h}_{j,k} \sim \mathcal{CN}(\boldsymbol{0},\sigma_{j,k}^2\boldsymbol{\Theta})$. Hence, different from $\boldsymbol{g}_{j,k}$, the entries in $\boldsymbol{h}_{j,k}$ are independent of each other. The correlated channel (1) is thus de-correlated by (9). Denote

$$p_{\text{out},k}^{\text{lb}}(r_k) = \Pr\left\{\frac{|h_{k,k}^{(1)}|}{|h_{\bar{k},k}^{(1)}|} < r_k,\ldots,\frac{|h_{k,k}^{(N)}|}{|h_{\bar{k},k}^{(N)}|} < r_k\right\}. \tag{11}$$

In the following theorem we analyze $p_{\text{out},k}^{\text{lb}}(r_k)$ and show that it is a lower bound to the outage probability $p_{\text{out},k}(r_k)$.

Theorem 1. *The outage probability $p_{out,k}(r_k)$ in (4) is lower bounded by $p^{lb}_{out,k}(r_k)$, where*

$$p^{lb}_{out,k}(r_k) = \left(\frac{r_k^2}{1+r_k^2}\right)^N. \tag{12}$$

Proof: See Appendix A. ∎

Remark 1. *As we explained in Appendix A, $p^{lb}_{out,k}(r_k)$ can be seen as the outage probability of the special case of (1) with no spatial correlation among ports and additive noise. In this idealized scenario, increasing the number of ports N provides each user with a greater number of alternatives in selecting a port with minimal interference. Therefore, as shown by (12), the outage probability experiences an exponential reduction with an increase in N. However, in practice, the N ports of a fluid antenna are evenly distributed within a limited linear space of length $W\lambda$ and the ports are correlated. Hence, with a fixed W, increasing N helps reduce the outage probability at the beginning, but then saturates since a smaller port distance causes strong inter-correlation. Accordingly, with a fixed N, if W increases, the distance between two adjacent ports gets larger and the outage probability approaches the lower bound $p^{lb}_{out,k}(r_k)$. We will further show this by simulations.* ◊

B. First-stage Approximation

Here, we show that the channel model $g^{(n)}_{j,k}$ in (6) can be approximated by taking only a few eigenvalues into account.

1) Channel Model Approximation: In (6), the exact channel model is mainly determined by $\boldsymbol{\Sigma}$, which on one hand, ensures $g^{(n)}_{j,k} \sim \mathcal{CN}(0, \sigma^2_{j,k})$, and on the other hand, determines the correlation of the elements in $\boldsymbol{g}_{j,k}$. In [32, Theorem 5], it is demonstrated that when N is large, the fraction of eigenvalues of $\boldsymbol{\Sigma}$ less than a small threshold approaches a constant that is independent of the threshold. Then, it is proposed to consider only ϵ-rank eigenvalues in the channel model, where (see [32, (19)])

$$\epsilon\text{-rank} \approx 2W\left(\frac{N}{N-1}\right). \tag{13}$$

In the following we study the property of the eigenvalues of $\boldsymbol{\Sigma}$ from another perspective and show that similar observations can be made as [32].

It can be found from (2) that the elements of $\boldsymbol{\Sigma}$ satisfy

$$\begin{aligned}(\boldsymbol{\Sigma})_{n,n'} &= (\boldsymbol{\Sigma})_{n',n} \\ &= (\boldsymbol{\Sigma})_{n+1,n'+1}, \text{ for } 1 \le n, n' \le N-1.\end{aligned} \tag{14}$$

$\boldsymbol{\Sigma}$ is thus a Hermitian Toeplitz matrix. Since a FAS usually has large numbers of ports, i.e., N is large, we prove later that $\theta_1 \gg \theta_N$ and only a few eigenvalues of $\boldsymbol{\Sigma}$ are significant. This makes it possible to approximate $g^{(n)}_{j,k}$ in (6) by taking only a few eigenvalues into account. Specifically, we consider $M \ll N$ terms in (6) with the largest eigenvalues, neglect the other terms, and obtain the following approximation

$$\tilde{g}^{(n)}_{j,k} = \sigma_{j,k}\sum_{m=1}^{M}\sqrt{\theta_m}u_{n,m}\left(a^{(m)}_{j,k} + ib^{(m)}_{j,k}\right). \tag{15}$$

By considering only M terms with dominant eigenvalues, which capture the most significant channel variations, we are able to reduce the complexity of the analysis while still maintaining reasonable accuracy. Then, a crucial question is to what extent $\tilde{g}^{(n)}_{j,k}$ can approximate $g^{(n)}_{j,k}$. To address this, we introduce a threshold θ_{th} for the eigenvalues of $\boldsymbol{\Sigma}$ and define the step function

$$H(\theta, \theta_{\text{th}}) \triangleq \begin{cases} 1, & \theta > \theta_{\text{th}}, \\ 0, & \theta \le \theta_{\text{th}}. \end{cases} \tag{16}$$

In addition, we define

$$\begin{cases} D_N(\theta_{\text{th}}) \triangleq \dfrac{1}{N}\displaystyle\sum_{n=1}^{N} H(\theta_n, \theta_{\text{th}}), \\ S_N(\theta_{\text{th}}) \triangleq \dfrac{1}{N}\displaystyle\sum_{n=1}^{N} \theta_n H(\theta_n, \theta_{\text{th}}). \end{cases} \tag{17}$$

Obviously, we can interpret $D_N(\theta_{\text{th}})$ as the proportion of eigenvalues greater than θ_{th} and $S_N(\theta_{\text{th}})$ as the average value of those eigenvalues. The limits of $D_N(\theta_{\text{th}})$ and $S_N(\theta_{\text{th}})$ are derived in the following theorem.

Theorem 2. *As the number of ports N grows large, the limits of $D_N(\theta_{th})$ and $S_N(\theta_{th})$ are, respectively, approximated as*

$$\lim_{N\to+\infty} D_N(\theta_{th}) \approx \frac{1}{2\pi}\int_{-\pi}^{\pi} \hat{H}(f(x), \theta_{th})dx, \tag{18}$$

$$\lim_{N\to+\infty} S_N(\theta_{th}) \approx \frac{1}{2\pi}\int_{-\pi}^{\pi} f(x)\hat{H}(f(x), \theta_{th})dx, \tag{19}$$

where $f(x)$, given in (44), is an exponential-form Fourier series, and $\hat{H}(f(x), \theta_{th})$, provided in (45), is a smooth approximation of the non-continuous step function $H(\theta, \theta_{th})$.

Proof: See Appendix B. ∎

In the following Table II, we compute the limits of D_N and S_N based on (18) and (19). Since $\sum_{n=1}^{N}\theta_n = \text{tr}(\boldsymbol{\Sigma}) = N$, which is large, we set $\theta_{\text{th}} = 1$. For comparison, the value of ϵ-rank$/N$ for different W is also provided in the table, where ϵ-rank is defined in (13). Note that when computing the limits of D_N and S_N, we consider a fixed Δ, i.e., fixed adjacent ports distance, since otherwise the elements of $\boldsymbol{\Sigma}$ vary with Δ (see (43)). Here we set $\Delta = W/99$, i.e., the distance between any two adjacent ports is fixed as if there are 100 ports.

TABLE II
LIMITS OF $D_N(1)$ AND $S_N(1)$, AND ϵ-RANK$/N$ FOR DIFFERENT W

W	0.5	1	2	3	4	5
Limit of $D_N(1)$	1.3%	2.3%	4.3%	6.3%	8.3%	10.4%
Limit of $S_N(1)$	0.9997	0.9996	0.9993	0.9990	0.9988	0.9996
ϵ-rank$/N$ in [32]	1.0%	2.0%	4.0%	6.1%	8.1%	10.1%

Table II illustrates that the limit of $D_N(1)$ is very small, indicating that only a small fraction of eigenvalues exceed 1. On the other hand, the limit of $S_N(1)$ is quite close to 1. This observation, combined with the fact that $\frac{1}{N}\sum_{n=1}^{N}\theta_n = 1$ suggests that the energy of $\boldsymbol{\Sigma}$ is concentrated in the largest few eigenvalues. Moreover, it can be seen that $D_N(1)$ is quite close to ϵ-rank$/N$. Therefore, with a sufficiently large N, $\tilde{g}^{(n)}_{j,k}$ in (15) can accurately approximate $g^{(n)}_{j,k}$ using a small M. We will further show this by simulations in Section IV.

To facilitate the analysis of outage probability, following the approach in [32], we introduce two additional variables $c_{j,k}^{(n)}$ and $d_{j,k}^{(n)}$, which are i.i.d. Gaussian variables with zero-mean and variance $\frac{1}{2}$, to $\tilde{g}_{j,k}^{(n)}$, and get

$$\hat{g}_{j,k}^{(n)} = \sigma_{j,k} \sum_{m=1}^{M} \sqrt{\theta_m} u_{n,m} \left(a_{j,k}^{(m)} + i b_{j,k}^{(m)} \right) + \sigma_{j,k} \sqrt{1 - \sum_{m=1}^{M} \theta_m u_{n,m}^2} \left(c_{j,k}^{(n)} + i d_{j,k}^{(n)} \right). \quad (20)$$

In contrast to $\tilde{g}_{j,k}^{(n)}$ given by (15), the new approximation $\hat{g}_{j,k}^{(n)}$ offers two advantages. First, its variance is precisely $\sigma_{j,k}^2$. Second, as we will demonstrate in the subsequent subsection, this approximation simplifies the analysis of the outage probability, making it more feasible to evaluate.

2) Outage Probability Analysis: According to (20), the outage probability of user k in (4) can be approximated as

$$\begin{aligned} p_{\text{out},k}(r_k) &\approx \Pr\left\{ \frac{|\hat{g}_{k,k}^{(1)}|}{|\hat{g}_{\bar{k},k}^{(1)}|} < r_k, \ldots, \frac{|\hat{g}_{k,k}^{(N)}|}{|\hat{g}_{\bar{k},k}^{(N)}|} < r_k \right\} \\ &= \Pr\left\{ \Phi_k^{(1)} < r_k, \ldots, \Phi_k^{(N)} < r_k \right\} \\ &= F_{\max\left\{\Phi_k^{(1)}, \ldots, \Phi_k^{(N)}\right\}}(r_k), \end{aligned} \quad (21)$$

where $\Phi_k^{(n)} = |\hat{g}_{k,k}^{(n)}|/|\hat{g}_{\bar{k},k}^{(n)}|$. In the following theorem, we provide the cumulative distribution function (CDF) of $\max\{\Phi_k^{(1)}, \ldots, \Phi_k^{(N)}\}$.

Theorem 3. *With the approximation $\hat{g}_{j,k}^{(n)}$ provided in (20), the CDF of $\max\left\{\Phi_k^{(1)}, \ldots, \Phi_k^{(N)}\right\}$ is given by (22) at the bottom of this page, where*

$$\begin{aligned} &F_{\Phi_k^{(n)}|(\boldsymbol{a}_{k,k}, \boldsymbol{a}_{\bar{k},k}, \boldsymbol{b}_{k,k}, \boldsymbol{b}_{\bar{k},k})}(r_k) \\ &= 1 - \int_0^{+\infty} Q_1\left(\sqrt{\frac{\alpha_{k,k}^{(n)}}{\beta_{k,k}^{(n)}}}, \frac{r_k z}{\sqrt{\beta_{k,k}^{(n)}}} \right) \frac{z}{\beta_{\bar{k},k}^{(n)}} \exp\left(-\frac{z^2 + \alpha_{\bar{k},k}^{(n)}}{2\beta_{\bar{k},k}^{(n)}} \right) \\ &\quad \times I_0\left(\frac{\sqrt{\alpha_{\bar{k},k}^{(n)}}}{\beta_{\bar{k},k}^{(n)}} z \right) dz, \end{aligned} \quad (23)$$

in which $Q_1(\cdot,\cdot)$ and $I_0(\cdot)$ are defined in Table I, and $\alpha_{j,k}^{(n)}$ as well as $\beta_{j,k}^{(n)}$ are given in (49).

Proof: See Appendix C. ∎

Based on (21) and Theorem 3, we could obtain an approximation of the FAMA system's outage probability $p_{\text{out},k}(r_k)$. To differentiate it from the scheme presented in the subsequent subsection, we regard this as the first-stage approximation.

C. Second-stage Approximation

By taking into account only M largest eigenvalues, the channel model $g_{j,k}^{(n)}$ in (6) has been significantly simplified by $\tilde{g}_{j,k}^{(n)}$ and $\hat{g}_{j,k}^{(n)}$ in the first stage. However, as shown by (22), the CDF expression $F_{\max\left\{\Phi_k^{(1)}, \ldots, \Phi_k^{(N)}\right\}}(r_k)$, which is an approximation of $p_{\text{out},k}(r_k)$, is still hard to compute as it is a $4M$-fold integral (let alone the integral (23)). Therefore, in this subsection we further approximate the distribution of $\hat{g}_{j,k}^{(n)}$ in (20) or $\hat{\boldsymbol{g}}_{j,k} = (\hat{g}_{j,k}^{(1)}, \ldots, \hat{g}_{j,k}^{(N)})^T$ using the strategy proposed in [32]. As in [32], we also call it second-stage approximation.

1) Channel Model Approximation: Here, we approximate $\hat{\boldsymbol{g}}_{j,k}$ in two steps. In the first step, we define a random matrix $\hat{\boldsymbol{G}}_{j,k}$ of size $N \times L$, where each column has the same distribution as $\hat{\boldsymbol{g}}_{j,k}$, while different columns are statistically independent. Therefore, $\hat{\boldsymbol{G}}_{j,k}$ can be seen as an L-dimensional extension of $\hat{\boldsymbol{g}}_{j,k}$. Here L is a key parameter that affects the approximation accuracy and has to be well designed. Then in the second step, we define another random matrix $\overline{\boldsymbol{G}}_{j,k}$ of the same size to approximate the distribution of $\hat{\boldsymbol{G}}_{j,k}$.

In particular, we define

$$\hat{g}_{j,k}^{n,l} = \sigma_{j,k} \sum_{m=1}^{M} \sqrt{\theta_m} u_{n,m} \left(\hat{a}_{j,k}^{m,l} + i \hat{b}_{j,k}^{m,l} \right) + \sigma_{j,k} \sqrt{1 - \sum_{m=1}^{M} \theta_m u_{n,m}^2} \left(\hat{c}_{j,k}^{n,l} + i \hat{d}_{j,k}^{n,l} \right), \quad (24)$$

and

$$\hat{\boldsymbol{G}}_{j,k} = \begin{bmatrix} \hat{g}_{j,k}^{1,1} & \hat{g}_{j,k}^{1,2} & \cdots & \hat{g}_{j,k}^{1,L} \\ \hat{g}_{j,k}^{2,1} & \hat{g}_{j,k}^{2,2} & \cdots & \hat{g}_{j,k}^{2,L} \\ \vdots & \vdots & \ddots & \vdots \\ \hat{g}_{j,k}^{N,1} & \hat{g}_{j,k}^{N,2} & \cdots & \hat{g}_{j,k}^{N,L} \end{bmatrix}, \quad (25)$$

where $\hat{a}_{j,k}^{m,l}$, $\hat{b}_{j,k}^{m,l}$, $\hat{c}_{j,k}^{n,l}$, and $\hat{d}_{j,k}^{n,l}$ are i.i.d. Gaussian variables with zero-mean and variance $\frac{1}{2}$. It can be seen from (24) that each $\hat{g}_{j,k}^{n,l}$ consists of $2(M+1)$ random variables, i.e., $(\hat{a}_{j,k}^{1,l}, \ldots, \hat{a}_{j,k}^{M,l})^T$, $(\hat{b}_{j,k}^{1,l}, \ldots, \hat{b}_{j,k}^{M,l})^T$, $\hat{c}_{j,k}^{n,l}$, and $\hat{d}_{j,k}^{n,l}$. The entries in the same column of $\hat{\boldsymbol{G}}_{j,k}$ share the same $(\hat{a}_{j,k}^{1,l}, \ldots, \hat{a}_{j,k}^{M,l})^T$ and $(\hat{b}_{j,k}^{1,l}, \ldots, \hat{b}_{j,k}^{M,l})^T$. Therefore, $\hat{\boldsymbol{G}}_{j,k}$ has dependent rows

$$\begin{aligned} &F_{\max\left\{\Phi_k^{(1)}, \ldots, \Phi_k^{(N)}\right\}}(r_k) \\ &= \frac{1}{\pi^{2M}} \int_{-\infty}^{+\infty} \cdots \int_{-\infty}^{+\infty} \exp\left\{ -\sum_{m=1}^{M} \left[\left(a_{k,k}^{(m)}\right)^2 + \left(a_{\bar{k},k}^{(m)}\right)^2 + \left(b_{k,k}^{(m)}\right)^2 + \left(b_{\bar{k},k}^{(m)}\right)^2 \right] \right\} \\ &\quad \times \prod_{n=1}^{N} F_{\Phi_k^{(n)}|(\boldsymbol{a}_{k,k}, \boldsymbol{a}_{\bar{k},k}, \boldsymbol{b}_{k,k}, \boldsymbol{b}_{\bar{k},k})}(r_k) \; da_{k,k}^{(1)} \cdots da_{k,k}^{(M)} da_{\bar{k},k}^{(1)} \cdots da_{\bar{k},k}^{(M)} db_{k,k}^{(1)} \cdots db_{k,k}^{(M)} db_{\bar{k},k}^{(1)} \cdots db_{\bar{k},k}^{(M)}, \end{aligned} \quad (22)$$

and each of its column has the same distribution as $\hat{\boldsymbol{g}}_{j,k}$. In addition, it can be found that all entries in $\hat{\boldsymbol{G}}_{j,k}$ use different $\hat{c}_{j,k}^{n,l}$ and $\hat{d}_{j,k}^{n,l}$, and distinct columns use different variables $(\hat{a}_{j,k}^{1,l},\ldots,\hat{a}_{j,k}^{M,l})^T$ and $(\hat{b}_{j,k}^{1,l},\ldots,\hat{b}_{j,k}^{M,l})^T$. Therefore, $\hat{\boldsymbol{G}}_{j,k}$ has independent columns and it can be seen as an L-dimensional extension of $\hat{\boldsymbol{g}}_{j,k}$.

Next, we define another random matrix $\overline{\boldsymbol{G}}_{j,k}$ of size $N\times L$ to approximate the distribution of $\hat{\boldsymbol{G}}_{j,k}$. In particular, we define

$$\overline{g}_{j,k}^{n,l}=\sigma_{j,k}\sum_{m=1}^{M}\sqrt{\theta_m}u_{n,m}\left(\overline{a}_{j,k}^{n,m}+i\overline{b}_{j,k}^{n,m}\right)+\sigma_{j,k}\sqrt{1-\sum_{m=1}^{M}\theta_m u_{n,m}^2}\left(\overline{c}_{j,k}^{n,l}+i\overline{d}_{j,k}^{n,l}\right), \quad (26)$$

and

$$\overline{\boldsymbol{G}}_{j,k}=\begin{bmatrix}\overline{g}_{j,k}^{1,1} & \overline{g}_{j,k}^{1,2} & \cdots & \overline{g}_{j,k}^{1,L}\\ \overline{g}_{j,k}^{2,1} & \overline{g}_{j,k}^{2,2} & \cdots & \overline{g}_{j,k}^{2,L}\\ \vdots & \vdots & \ddots & \vdots\\ \overline{g}_{j,k}^{N,1} & \overline{g}_{j,k}^{N,2} & \cdots & \overline{g}_{j,k}^{N,L}\end{bmatrix}. \quad (27)$$

We see from (26) that all entries in $\overline{\boldsymbol{G}}_{j,k}$ use different $\overline{c}_{j,k}^{n,l}$ and $\overline{d}_{j,k}^{n,l}$, and the entries in the same row share the same $(\overline{a}_{j,k}^{n,1},\ldots,\overline{a}_{j,k}^{n,M})^T$ and $(\overline{b}_{j,k}^{n,1},\ldots,\overline{b}_{j,k}^{n,M})^T$. Therefore, different from $\hat{\boldsymbol{G}}_{j,k}$, $\overline{\boldsymbol{G}}_{j,k}$ has independent rows and dependent columns. As we will show below, the introduction of the new random matrix $\overline{\boldsymbol{G}}_{j,k}$ makes the analysis of the outage probability much more manageable.

To ensure an effective approximation of $\hat{\boldsymbol{G}}_{j,k}$ by $\overline{\boldsymbol{G}}_{j,k}$, it is essential to determine a well-designed parameter L. As in [32], we vectorize both $\hat{\boldsymbol{G}}_{j,k}$ and $\overline{\boldsymbol{G}}_{j,k}$, and minimize the distance between the covariance matrices of the obtained vectors by optimizing L. Then, according to [32, Theorem 8], we have

$$L=\min\left\{\left\lfloor\frac{1.52(N-1)}{2\pi W}\right\rfloor,N\right\}, \quad (28)$$

where $\lfloor\cdot\rfloor$ is the floor function.

2) Outage Probability Analysis: Now we analyze the outage probability of the considered FAMA system based on the new approximation. First, we define

$$\begin{cases}\hat{\Phi}_k^{n,l}=\dfrac{|\hat{g}_{k,k}^{n,l}|}{|\hat{g}_{\bar{k},k}^{n,l}|},\\ \hat{\Psi}_k=\max\left\{\hat{\Phi}_k^{n,l},1\le n\le N,1\le l\le L\right\}.\end{cases} \quad (29)$$

Since $\hat{\boldsymbol{G}}_{j,k},\forall j,k\in\{1,2\}$ has L independent columns and each column has the same distribution as $\hat{\boldsymbol{g}}_{j,k}$, the CDF of $\hat{\Psi}_k$ can be expressed as

$$\begin{aligned}F_{\hat{\Psi}_k}(r_k)&=\Pr\left\{\hat{\Phi}_k^{n,l}<r_k,1\le n\le N,1\le l\le L\right\}\\&=\prod_{l=1}^{L}\Pr\left\{\hat{\Phi}_k^{1,l}<r_k,\cdots,\hat{\Phi}_k^{N,l}<r_k\right\}\\&=\left[F_{\max\left\{\Phi_k^{(1)},\ldots,\Phi_k^{(N)}\right\}}(r_k)\right]^L,\end{aligned} \quad (30)$$

where $F_{\max\left\{\Phi_k^{(1)},\ldots,\Phi_k^{(N)}\right\}}(r_k)$ is the first-stage approximation of the outage probability given in (21). Furthermore, we define

$$\begin{cases}\overline{\Phi}_k^{n,l}=\dfrac{|\overline{g}_{k,k}^{n,l}|}{|\overline{g}_{\bar{k},k}^{n,l}|},\\ \overline{\Psi}_k=\max\left\{\overline{\Phi}_k^{n,l},1\le n\le N,1\le l\le L\right\}.\end{cases} \quad (31)$$

Since $\overline{\boldsymbol{G}}_{j,k},\forall j,k\in\{1,2\}$ has independent rows, the CDF of $\hat{\Psi}_k$ is

$$\begin{aligned}F_{\overline{\Psi}_k}(r_k)&=\Pr\left\{\overline{\Phi}_k^{n,l}\le r_k,1\le n\le N,1\le l\le L\right\}\\&=\prod_{n=1}^{N}\Pr\left\{\overline{\Phi}_k^{n,l}\le r_k,1\le l\le L\right\}.\end{aligned} \quad (32)$$

In the following theorem, we provide the closed-form expression of $F_{\overline{\Psi}_k}(r_k)$.

Theorem 4. *According to the above definitions, the CDF of $\overline{\Psi}_k$ can be computed as*

$$\begin{aligned}&F_{\overline{\Psi}_k}(r_k)\\&=\prod_{n=1}^{N}\frac{1}{\sigma_{k,k}^2\sigma_{\bar{k},k}^2\xi_n^2}\int_0^{+\infty}\int_0^{+\infty}\exp\left(-\frac{\alpha_1}{\sigma_{k,k}^2\xi_n}-\frac{\alpha_2}{\sigma_{\bar{k},k}^2\xi_n}\right)\\&\times\left[1-\int_0^{+\infty}Q_1\left(\sqrt{\frac{\alpha_1}{\overline{\beta}_{k,k}^{(n)}}},\frac{r_k z}{\sqrt{\overline{\beta}_{k,k}^{(n)}}}\right)\frac{z}{\overline{\beta}_{\bar{k},k}^{(n)}}\exp\left(-\frac{z^2+\alpha_2}{2\overline{\beta}_{\bar{k},k}^{(n)}}\right)\right.\\&\left.\times I_0\left(\frac{\sqrt{\alpha_2}}{\overline{\beta}_{\bar{k},k}^{(n)}}z\right)dz\right]^L d\alpha_1 d\alpha_2,\end{aligned} \quad (33)$$

where $\xi_n=\sum_{m=1}^{M}\theta_m u_{n,m}^2$ and $\overline{\beta}_{j,k}^{(n)}=\frac{\sigma_{j,k}^2}{2}(1-\xi_n)$.

Proof: See Appendix D. ∎

Since $\overline{\boldsymbol{G}}_{j,k}$ approximates $\hat{\boldsymbol{G}}_{j,k}$, according to (21), (30), and Theorem 4, we can get the second-stage approximation of the outage probability as

$$\begin{aligned}p_{\text{out},k}(r_k)&\approx F_{\max\left\{\Phi_k^{(1)},\ldots,\Phi_k^{(N)}\right\}}(r_k)\\&=\left[F_{\hat{\Psi}_k}(r_k)\right]^{\frac{1}{L}}\\&\approx\left[F_{\overline{\Psi}_k}(r_k)\right]^{\frac{1}{L}}.\end{aligned} \quad (34)$$

Theorem 5. *If M is large enough such that $\xi_n\to 1$, the CDF of $\overline{\Psi}_k$ can be approximated as*

$$F_{\overline{\Psi}_k}(r_k)\approx\left(\frac{r_k^2}{1+r_k^2}\right)^N. \quad (35)$$

Proof: See Appendix E. ∎

IV. Results and Discussions

In this section, we present simulation results to evaluate the performance of the two-user slow FAMA system, and study the accuracy of the proposed lower bound as well as the approximation schemes. For convenience, we assume equal transmit power for both BS antennas, i.e., $p_1=p_2$. In addition, we assume equal large-scale fading from different BS antennas

This article has been accepted for publication in IEEE Transactions on Wireless Communications. This is the author's version which has not been fully edited and content may change prior to final publication. Citation information: DOI 10.1109/TWC.2024.3363499

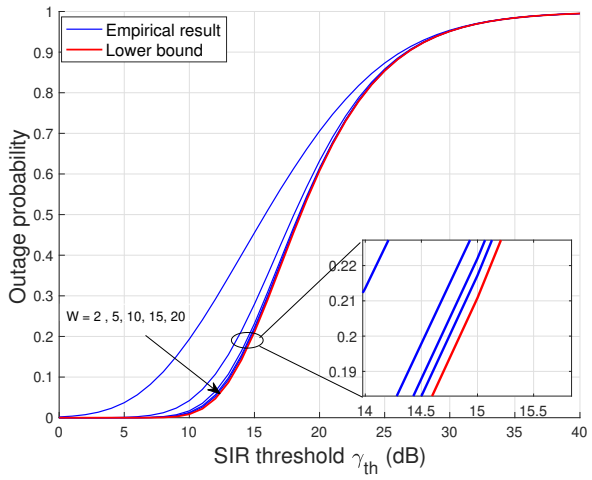

Fig. 2. Outage probability versus γ_{th} with $N = 50$.

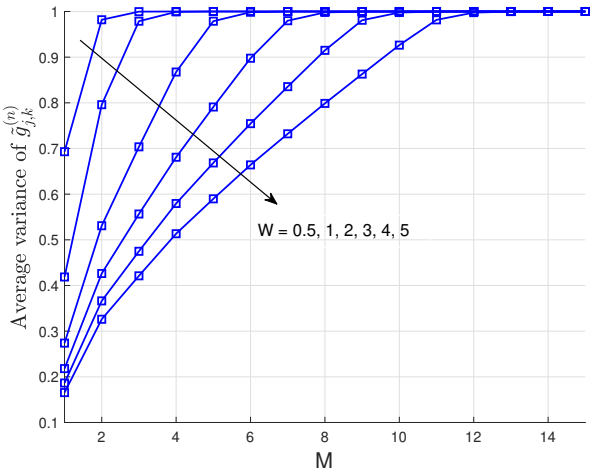

Fig. 4. Average variance of $\tilde{g}_{j,k}^{(n)}, \forall n \in \{1, \ldots, N\}$ versus the approximation level M with $N = 100$.

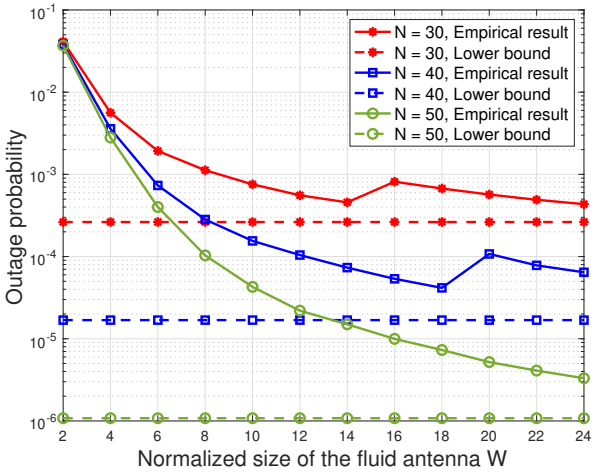

Fig. 3. Outage probability versus W with $\gamma_{\text{th}} = 5$ dB.

to the same user, i.e., $\sigma_{1,k} = \sigma_{2,k}$. Then, it is obvious from (4) that $\sigma_{j,k}$ does not affect the value of the outage probability. Thus, we simply set $\sigma_{1,k} = \sigma_{2,k} = 1$. We assume that the FAS operates at frequency of 5GHz with a wavelength $\lambda = 6$cm [9]. It is thus reasonable to consider W in the interval $[0, 5]$, i.e., the size of a FAS on the user side (mobile phone or laptop) varies from 0 to 30cm. In most figures in the simulation, we consider $W \in [0, 5]$. However, in some cases, to observe a trend in the outage probability or to see the performance of the proposed approximation schemes under more configurations, we also show large W. For example, in Fig. 2, by varying W from 2 to 20, we see that the outage probability quickly approaches the lower bound as W increases.

In the following simulation, some results are obtained based on the closed-form expressions, e.g., the lower bound (12) and the second-stage approximation of the outage probability (5). Some results are obtained using Monte Carlo simulations by averaging over 10^8 independent channel realizations. For example, the empirical value of the outage probability is obtained by Monte Carlo simulation based on the exact channel model $g_{j,k}^{(n)}$ given in (6).

A. Lower Bound on the Outage Probability

In Fig. 2 and Fig. 3, we compare the empirical results of the FAMA system's outage probability with the lower bound. It can be seen from these two figures that when the normalized size of the fluid antenna W is large, the empirical curves get quite close to the lower bound. This is because, as shown in Appendix A, the lower bound can be seen as the outage probability of an idealized FAMA system with no spatial correlation among ports and additive noise. For a true FAMA system, when N is fixed and W increases, the distance between two adjacent ports gets larger and the correlation between any two ports diminishes. The empirical results thus approach the lower bound in this case. Moreover, Fig. 3 shows that when $N = 30$ and $N = 40$, the empirical results generally decrease with W, but the monotonicity of the curves vary at some points. This is because the channel model is generated based on the Jake's model. As shown in (2), this model involves the zero-order Bessel function of the first kind $J_0(\cdot)$, whose amplitude is not strictly monotonically decreasing with respect to the variable. Therefore, in cases where the value of W is large and its increment is relatively small, it is possible for the empirical curves to exhibit oscillations.

B. First-stage Approximation

In this subsection, we investigate the performance of the first-stage approximation. It should be noticed that although the channel model $g_{j,k}^{(n)}$ in (6) has been significantly simplified by $\hat{g}_{j,k}^{(n)}$, the CDF expression in Theorem 3 is still hard to compute as it is a $4M$-fold integral (let alone the integral (23)). Therefore, we obtain the first-stage approximation of the outage probability based on the channel models $\tilde{g}_{j,k}^{(n)}$ and $\hat{g}_{j,k}^{(n)}$ in (15) and (20) by Monte Carlo simulations.

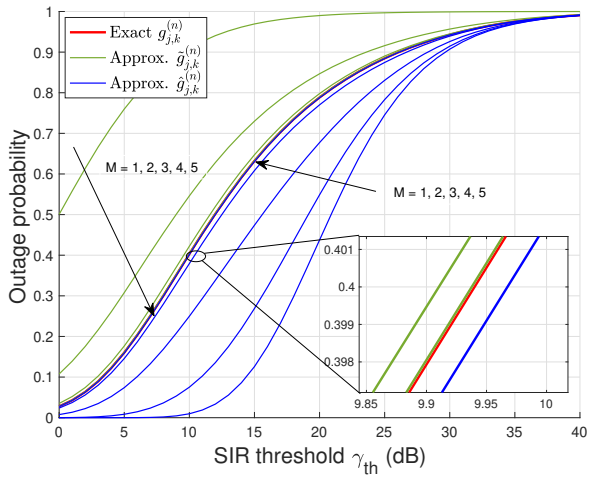

Fig. 5. Outage probability based on $g_{j,k}^{(n)}$, $\tilde{g}_{j,k}^{(n)}$, and $\hat{g}_{j,k}^{(n)}$ versus the SIR threshold γ_{th} with $W = 1$ and $N = 100$.

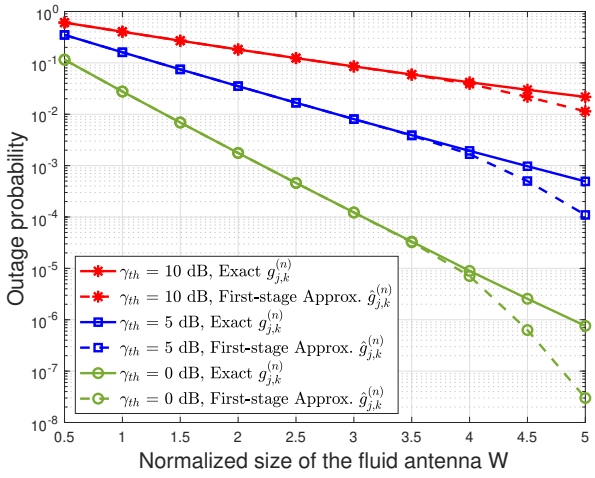

Fig. 7. Outage probability and the first-stage approximation versus W with $N = 100$ and $M = 10$.

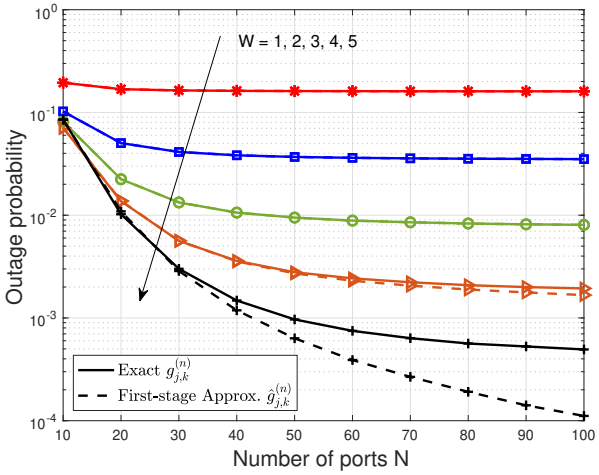

Fig. 6. Outage probability and the first-stage approximation versus N with $\gamma_{\text{th}} = 5$ dB and $M = 10$.

It is known from (15) that $\tilde{g}_{j,k}^{(n)} \sim \mathcal{CN}(0, \sum_{m=1}^{M} \theta_m u_{n,m}^2)$. Fig. 4 depicts the value of

$$\frac{1}{N}\sum_{n=1}^{N} \text{Cov}\left[\tilde{g}_{j,k}^{(n)}\right] = \frac{1}{N}\sum_{n=1}^{N}\sum_{m=1}^{M} \theta_m u_{n,m}^2, \tag{36}$$

which can be seen as the average variance of $\tilde{g}_{j,k}^{(n)}, \forall n \in \{1, \ldots, N\}$. Note that in the extreme $M = N$ case, the value of (36) is 1 since $\sum_{m=1}^{N} \theta_m u_{n,m}^2 = 1$ (see (7)). Therefore, when M is smaller than N and increases, the value of (36) should gradually approach 1. Fig. 4 shows that this is true and can be realized by a small M (in contrast to N). For example, when $W = 0.5$ and $W = 2$, the value of (36) is close to 1 with M, respectively, being 3 and 6. Therefore, the exact channel model $g_{j,k}^{(n)}$ in (6) can be accurately approximated by taking into account only a few eigenvalues of $\boldsymbol{\Sigma}$. This is consistent with the observation in Table II.

Fig. 5 illustrates the outage probability using the exact channel model $g_{j,k}^{(n)}$, as well as its approximations $\tilde{g}_{j,k}^{(n)}$ and $\hat{g}_{j,k}^{(n)}$. It can be observed that compared to the curve obtained from $g_{j,k}^{(n)}$, the outage probability resulting from $\tilde{g}_{j,k}^{(n)}$ and $\hat{g}_{j,k}^{(n)}$ respectively serve as upper and lower bounds. As M increases, the bounds approach quickly to the curve obtained from $g_{j,k}^{(n)}$. The approximation is considered sufficiently accurate when $M = 4$ (with $W = 1$ and $N = 100$), which aligns with the observations in Fig. 4. Since both $\tilde{g}_{j,k}^{(n)}$ and $\hat{g}_{j,k}^{(n)}$ can provide good approximations of $g_{j,k}^{(n)}$, and it is more convenient to analyze the outage probability based on $\hat{g}_{j,k}^{(n)}$, we only plot the curves for $g_{j,k}^{(n)}$ and $\hat{g}_{j,k}^{(n)}$ in the subsequent Figs. 6 and 7.

Figs. 6 and 7 provide insights into the impact of N and W on the outage probability. Several observations can be made. First, when W is small, e.g., $W = 1$, the outage probability remains almost constant as N increases. In contrast, when W is large, the outage probability first decreases greatly with N and then saturates. This is because the antenna ports are highly correlated. With a fixed W, increasing N initially helps reduce the outage probability by introducing additional diversity. However, as N becomes large, the benefits of increased N diminish due to the stronger inter-correlation resulting from smaller port distances. Secondly, for a given N, the system's outage probability decreases exponentially with W. But this is not always true. In fact, as demonstrated in Fig. 3, for a given N, when W becomes sufficiently large, the outage probability approaches the derived lower bound. Furthermore, both Fig. 6 and Fig. 7 highlight an interesting observation regarding the approximation level M. When W is small, the solid and dashed lines completely coincide, indicating that the approximation scheme using $\hat{g}_{j,k}^{(n)}$ with $M = 10$ is sufficient for accurate results. However, when W becomes larger, for example, $W = 4.5$ or $W = 5$, the outage probability obtained using $\hat{g}_{j,k}^{(n)}$ is noticeably smaller than that resulted from $g_{j,k}^{(n)}$. This discrepancy arises because we set the approximation level

This article has been accepted for publication in IEEE Transactions on Wireless Communications. This is the author's version which has not been fully edited and content may change prior to final publication. Citation information: DOI 10.1109/TWC.2024.3363499

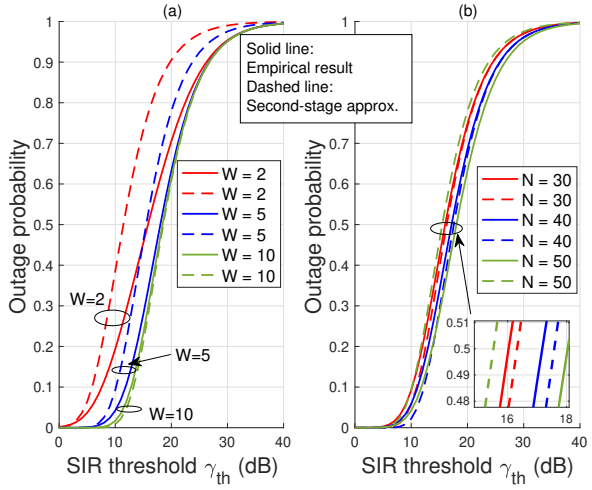

Fig. 8. Empirical CDF versus the second-stage approximation of the outage probability with (a). $N = 50$ and $M = 10$; (b). $W = 5$ and $M = 10$.

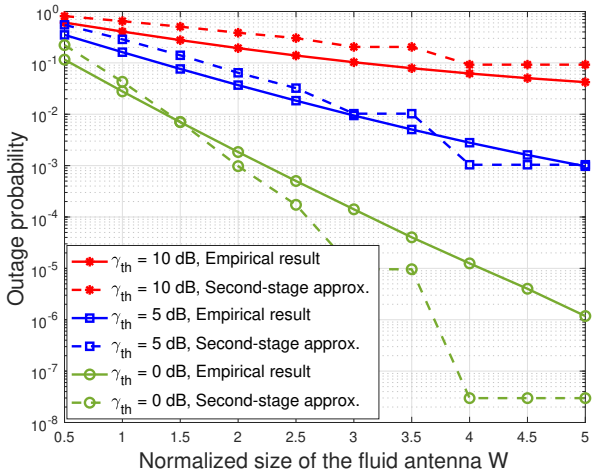

Fig. 10. Outage probability and the second-stage approximation versus W with $N = 50$ and $M = 10$.

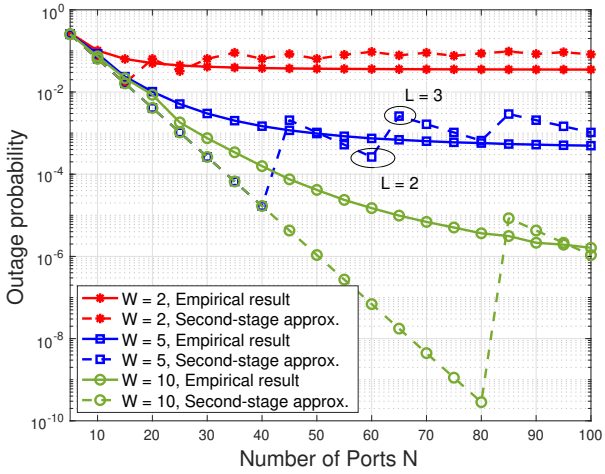

Fig. 9. Outage probability and the second-stage approximation versus N with $\gamma_{\text{th}} = 5$ dB and $M = 10$.

M to be 10 for all configurations. It is known from Fig. 4 that this is adequate to accurately represent the channel behavior when W is smaller than 4. However, when $W = 5$, a higher approximation level, such as $M = 12$, is necessary to ensure that the value of (36) approaches 1. In this case, the outage probability obtained from $\hat{g}_{j,k}^{(n)}$ is a lower bound to that based on $g_{j,k}^{(n)}$, which is also demonstrated by Fig. 5.

C. Second-stage Approximation

Now we investigate the performance of the second strategy in approximating the outage probability. Fig. 8 compares the empirical CDF with the second-stage approximation over the SIR threshold γ_{th}. Different values of M and N are also investigated. It is evident that the curves approximated through the second strategy are not as accurate as those obtained by the first strategy. However, they still exhibit a commendable level of similarity with the empirical curves, especially when W is relatively large (e.g., $W = 10$) or when N is of medium size (e.g., $N = 30$ or 40). The difference in performance between the first and second strategies stems from the fact that they approximate the channel model in different ways. In the first stage, the channel model $g_{j,k}^{(n)}$ is approximated by $\tilde{g}_{j,k}^{(n)}$ or $\hat{g}_{j,k}^{(n)}$ by only considering the largest M eigenvalues. Hence, for a fixed N, with a well-designed M, this scheme performs quite well. In the extreme case with $M = N$, it can be easily seen from (6), (15), and (20) that $g_{j,k}^{(n)} = \tilde{g}_{j,k}^{(n)} = \hat{g}_{j,k}^{(n)}$. Obviously, the first-stage approximation of the outage probability in this case is exactly the true one. Despite this advantage, as shown in Theorem 3, it is a $4M$-fold integral, which is difficult to compute and makes further analysis complicated. To address this problem, the second scheme first constructs a random matrix $\hat{\boldsymbol{G}}_{j,k}$, whose columns have the same distribution as $\hat{\boldsymbol{g}}_{j,k}$, and then proposes another random matrix $\overline{\boldsymbol{G}}_{j,k}$ to approximate $\hat{\boldsymbol{G}}_{j,k}$. The similarity between $\overline{\boldsymbol{G}}_{j,k}$ and $\hat{\boldsymbol{G}}_{j,k}$ is characterized using the distance between their covariance matrices, which is minimized by designing L [32]. This approximation (from $\hat{\boldsymbol{G}}_{j,k}$ to $\overline{\boldsymbol{G}}_{j,k}$) makes the formulation of the outage probability easier to compute, but compromises the performance slightly.

Figs. 9 and 10 investigate the impact of N and W on the outage probability. Similar observations about the performance of the two-user FAMA system, e.g., the relationship between the outage probability and N as well as W, can be made from the empirical results as Figs. 6 and 7. It can also be seen that when the outage probability is above 10^{-6}, the second strategy exhibits a good approximation performance. Another interesting observation is that unlike the empirical result, the approximation curves are not smooth and approximate the empirical curves in a regressive manner. This is because the approximation is obtained as follows (see (34))

$$p_{\text{out},k}(r_k) \approx \left[F_{\overline{\Psi}_k}(r_k)\right]^{\frac{1}{L}}, \tag{37}$$

where $F_{\overline{\Psi}_k}(r_k)$ is given in Theorem 4. Though $F_{\overline{\Psi}_k}(r_k)$ varies smoothly with N and M, the value of L does not. Since $L =$

$\min\left\{\left\lfloor\frac{1.52(N-1)}{2\pi W}\right\rfloor, N\right\}$[3], L generally increases with N and decreases with W. Due to the floor function $\lfloor\cdot\rfloor$, the value of L may change abruptly and this makes the curves unsmooth. For example, as shown in Fig. 9, when $W=5$ and N changes from 60 to 65, the value of L increases from 2 to 3, and this causes an obvious increase in $\left[F_{\overline{\Psi}_k}(r_k)\right]^{\frac{1}{L}}$. After that, as N continues to increase to 80, the value of L remains fixed at 3. Hence, as shown by Fig. 9, $\left[F_{\overline{\Psi}_k}(r_k)\right]^{\frac{1}{L}}$ decreases with N in this interval ($65 \le N \le 80$).

V. Conclusions

This paper presented an investigation into the outage performance of a downlink slow FAMA system with two users. The study focused on a fully correlated channel model that effectively captures the correlation between any two ports of the fluid antenna. In order to simplify the analysis, it was demonstrated that each channel coefficient could be adequately approximated by the M largest eigenvalues, in which M is considerably smaller than N. By employing this approximation, the outage probability can be expressed as a $4M$-fold integral. To further simplify the expression, we extended the second-stage approximation scheme for the single-user FAS in [32] to the considered FAMA system. Using this new model, another approximation of the outage probability was obtained, which involves a 2-fold integral and is easy to compute and more insightful. Simulation results have validated the approximation and demonstrated remarkable outage performance of the FAMA scheme. It is worth mentioning that although the second-stage approximation can help greatly simplify the analysis, its performance in approximating the channel model under some configurations is not as good as the first one. Therefore, further investigation is needed to explore alternative modeling approaches and achieve a more accurate approximation of the channel model.

Appendix A
Proof of Theorem 1

It is known from (10) that

$$\frac{|h_{k,k}^{(n)}|}{|h_{\bar{k},k}^{(n)}|} = \frac{\sigma_{k,k}\sqrt{\theta_n}|x_{k,k}^{(n)}|}{\sigma_{\bar{k},k}\sqrt{\theta_n}|x_{\bar{k},k}^{(n)}|} = \frac{|x_{k,k}^{(n)}|}{|x_{\bar{k},k}^{(n)}|}, \tag{38}$$

where the last step follows from the assumption that $\sigma_{k,k} = \sigma_{\bar{k},k}$. Since for all $1 \le j \le K$ and $1 \le n \le N$, $x_{j,k}^{(n)}$ are independent of each other and $|x_{j,k}^{(n)}| \sim \text{Rayleigh}(\frac{1}{\sqrt{2}})$, $p_{\text{out},k}^{\text{lb}}(r_k)$ in (11) can be rewritten as

$$p_{\text{out},k}^{\text{lb}}(r_k) = \Pr\left\{\frac{|x_{k,k}^{(1)}|}{|x_{\bar{k},k}^{(1)}|} < r_k, \ldots, \frac{|x_{k,k}^{(N)}|}{|x_{\bar{k},k}^{(N)}|} < r_k\right\} = \Pr\left\{\frac{\hat{X}}{X} < r_k\right\}^N, \tag{39}$$

[3]Note that if $\left\lfloor\frac{1.52(N-1)}{2\pi W}\right\rfloor = 0$, we force L to be 1

where $\hat{X}, X \sim \text{Rayleigh}(\frac{1}{\sqrt{2}})$ and they are independent. It is obvious from (39) that $p_{\text{out},k}^{\text{lb}}(r_k)$ can be seen as the outage probability of the following channel

$$\tilde{\boldsymbol{y}}_k = \sum_{j=1}^{2} \boldsymbol{x}_{j,k} s_j. \tag{40}$$

In contrast to (8), the channel in (40) has uncorrelated channel coefficients and no additive noise. Obviously, (40) can be seen as a special case of (1) with no noise and far-apart ports such that the channel gains at different ports are uncorrelated. Therefore, its outage probability $p_{\text{out},k}^{\text{lb}}(r_k)$ is a lower bound to $p_{\text{out},k}(r_k)$. Now the result (12) can be proven by

$$\begin{aligned}\Pr\left\{\frac{\hat{X}}{X} < r_k\right\} &= \Pr\left\{\hat{X} < r_k X\right\} \\ &= \int_0^{+\infty} F_{\hat{X}}(r_k x) f_X(x) dx \\ &\overset{(a)}{=} \int_0^{+\infty} \left(1 - e^{-r_k^2 x^2}\right) 2x e^{-x^2} dx \\ &= 1 - 2\int_0^{+\infty} x e^{-(1+r_k^2)x^2} dx \\ &= \frac{r_k^2}{1+r_k^2},\end{aligned} \tag{41}$$

where (a) follows from using the fact that $\hat{X}, X \sim \text{Rayleigh}(\frac{1}{\sqrt{2}})$ and their probability density function (PDF) as well as CDF. Combining (39) and (41), we then get (12).

Appendix B
Proof of Theorem 2

Since $\boldsymbol{\Sigma}$ is a Hermitian Toeplitz matrix, it can be found as

$$\boldsymbol{\Sigma} = \begin{bmatrix} \phi_0 & \phi_1 & \cdots & \phi_{N-1} \\ \phi_1 & \phi_0 & \ddots & \vdots \\ \vdots & \ddots & \ddots & \phi_1 \\ \phi_{N-1} & \cdots & \phi_1 & \phi_0 \end{bmatrix}. \tag{42}$$

According to (2) and [32, (47)], the coefficient ϕ_n can be represented in the following Fourier form

$$\begin{aligned}\phi_n &= J_0(2\pi n \Delta) \\ &= \frac{1}{2\pi}\int_{-\pi}^{\pi} e^{i2\pi n\Delta \sin x} dx \\ &= \frac{1}{2\pi}\int_{-\pi}^{\pi} f(x) e^{-inx} dx, \text{ for } n = 0, \ldots, N-1,\end{aligned} \tag{43}$$

where

$$f(x) = \sum_{m=-\infty}^{m=+\infty} J_0(2\pi m\Delta) e^{imx}, \ \forall x \in [-\pi, \pi], \tag{44}$$

is a real and integrable function.

Then we apply [37, Theorem 1.1] to evaluate the limiting distribution of $D_N(\theta_{\text{th}})$ and $S_N(\theta_{\text{th}})$. Note that [37, Theorem 1.1] requires $H(\theta, \theta_{\text{th}})$ to be a continuous function. Thus, we replace $H(\theta, \theta_{\text{th}})$ by a smooth and analytic approximation.

There are different ways to approximate a step function. Here we adopt the logistic function

$$\hat{H}(\theta,\theta_{\text{th}})=\frac{1}{1+e^{-2t(\theta-\theta_{\text{th}})}}, \tag{45}$$

as an approximation of $H(\theta,\theta_{\text{th}})$, where a larger t corresponds to a sharper transition at $\theta=\theta_{\text{th}}$. Then we have

$$\begin{aligned}\lim_{N\to+\infty} D_N(\theta_{\text{th}}) &= \lim_{N\to+\infty}\frac{1}{N}\sum_{n=1}^{N} H(\theta_n,\theta_{\text{th}})\\ &\approx \lim_{N\to+\infty}\frac{1}{N}\sum_{n=1}^{N}\hat{H}(\theta_n,\theta_{\text{th}})\\ &= \frac{1}{2\pi}\int_{-\pi}^{\pi}\hat{H}(f(x),\theta_{\text{th}})dx,\end{aligned} \tag{46}$$

where the last step follows by using [37, Theorem 1.1]. Hence, (18) is true. Analogously, based on the definition of $S_N(\theta_{\text{th}})$ in (17) and (45), (19) can be proven by following similar steps.

Appendix C
Proof of Theorem 3

For convenience, we denote $\boldsymbol{a}_{j,k}=(a_{j,k}^{(1)},\ldots,a_{j,k}^{(M)})^T$ and $\boldsymbol{b}_{j,k}=(b_{j,k}^{(1)},\ldots,b_{j,k}^{(M)})^T$. It is known from (20) that $\hat{g}_{j,k}^{(n)}$ is a Gaussian variable, and for a given $(\boldsymbol{a}_{j,k},\boldsymbol{b}_{j,k})$, it follows

$$\begin{aligned}\hat{g}_{j,k|(\boldsymbol{a}_{j,k},\boldsymbol{b}_{j,k})}^{(n)} \sim \mathcal{CN}\Bigg(&\sigma_{j,k}\sum_{m=1}^{M}\sqrt{\theta_m}u_{n,m}\left(a_{j,k}^{(m)}+ib_{j,k}^{(m)}\right),\\ &\sigma_{j,k}^2\left(1-\sum_{m=1}^{M}\theta_m u_{n,m}^2\right)\Bigg).\end{aligned} \tag{47}$$

Hence, $|\hat{g}_{j,k|(\boldsymbol{a}_{j,k},\boldsymbol{b}_{j,k})}^{(n)}|$ follows Rice or Rician distribution as shown below

$$\left|\hat{g}_{j,k|(\boldsymbol{a}_{j,k},\boldsymbol{b}_{j,k})}^{(n)}\right| \sim \text{Rice}\left(\sqrt{\alpha_{j,k}^{(n)}},\sqrt{\beta_{j,k}^{(n)}}\right), \tag{48}$$

where

$$\begin{cases}\alpha_{j,k}^{(n)}=\sigma_{j,k}^2\left[\left(\sum_{m=1}^{M}\sqrt{\theta_m}u_{n,m}a_{j,k}^{(m)}\right)^2+\left(\sum_{m=1}^{M}\sqrt{\theta_m}u_{n,m}b_{j,k}^{(m)}\right)^2\right],\\ \beta_{j,k}^{(n)}=\dfrac{\sigma_{j,k}^2}{2}\left(1-\sum_{m=1}^{M}\theta_m u_{n,m}^2\right).\end{cases} \tag{49}$$

Based on (48), we have

$$\begin{cases}\left|\hat{g}_{k,k|(\boldsymbol{a}_{k,k},\boldsymbol{b}_{k,k})}^{(n)}\right| \sim \text{Rice}\left(\sqrt{\alpha_{k,k}^{(n)}},\sqrt{\beta_{k,k}^{(n)}}\right),\\ \left|\hat{g}_{\bar{k},k|(\boldsymbol{a}_{\bar{k},k},\boldsymbol{b}_{\bar{k},k})}^{(n)}\right| \sim \text{Rice}\left(\sqrt{\alpha_{\bar{k},k}^{(n)}},\sqrt{\beta_{\bar{k},k}^{(n)}}\right).\end{cases} \tag{50}$$

Note that $|\hat{g}_{k,k}^{(n)}|$ and $|\hat{g}_{\bar{k},k}^{(n)}|$ are independent. Then for user k, $\Phi_k^{(n)}$ conditioned on $(\boldsymbol{a}_{k,k},\boldsymbol{a}_{\bar{k},k},\boldsymbol{b}_{k,k},\boldsymbol{b}_{\bar{k},k})$ is the ratio of two independent Rice random variables. We now derive its CDF. For convenience, we consider two independent Rician variables $\hat{Z}\sim\text{Rice}(\sqrt{\alpha_1},\sqrt{\beta_1})$, $Z\sim\text{Rice}(\sqrt{\alpha_2},\sqrt{\beta_2})$, and denote $R=\hat{Z}/Z$. Then the CDF of R can be derived as

$$\begin{aligned}&F_R(r)\\ &=\int_0^{+\infty}F_{\hat{Z}}(rz)f_Z(z)dz\\ &=1-\int_0^{+\infty}Q_1\left(\sqrt{\frac{\alpha_1}{\beta_1}},\frac{rz}{\sqrt{\beta_1}}\right)\frac{z}{\beta_2}\exp\left(-\frac{z^2+\alpha_2}{2\beta_2}\right)I_0\left(\frac{\sqrt{\alpha_2}}{\beta_2}z\right)dz,\end{aligned} \tag{51}$$

where the last step follows from the CDF and PDF of Rice distribution, $Q_1(\cdot,\cdot)$ is the Marcum Q-function of order 1, and $I_0(\cdot)$ is the modified Bessel function of the first kind. Using (51), the CDF $F_{\Phi_k^{(n)}|(\boldsymbol{a}_{k,k},\boldsymbol{a}_{\bar{k},k},\boldsymbol{b}_{k,k},\boldsymbol{b}_{\bar{k},k})}(r_k^{(n)})$ can be obtained directly using (23). For a given $(\boldsymbol{a}_{k,k},\boldsymbol{a}_{\bar{k},k},\boldsymbol{b}_{k,k},\boldsymbol{b}_{\bar{k},k})$, (20) indicates that $\Phi_k^{(n)},\forall n\in\{1,\ldots,N\}$ are independent of each other. Therefore, we have

$$\begin{aligned}&F_{(\Phi_k^{(1)},\ldots,\Phi_k^{(N)})|(\boldsymbol{a}_{k,k},\boldsymbol{a}_{\bar{k},k},\boldsymbol{b}_{k,k},\boldsymbol{b}_{\bar{k},k})}(r_k^{(1)},\ldots,r_k^{(N)})\\ &\qquad=\prod_{n=1}^{N}F_{\Phi_k^{(n)}|(\boldsymbol{a}_{k,k},\boldsymbol{a}_{\bar{k},k},\boldsymbol{b}_{k,k},\boldsymbol{b}_{\bar{k},k})}(r_k^{(n)}).\end{aligned} \tag{52}$$

The joint CDF of $(\Phi_k^{(1)},\ldots,\Phi_k^{(N)})$ is thus the expectation of (52) over $(\boldsymbol{a}_{k,k},\boldsymbol{a}_{\bar{k},k},\boldsymbol{b}_{k,k},\boldsymbol{b}_{\bar{k},k})$ and is given in (53) at the bottom of this page. Since

$$F_{\max\left\{\Phi_k^{(1)},\ldots,\Phi_k^{(N)}\right\}}(r_k)=F_{(\Phi_k^{(1)},\ldots,\Phi_k^{(N)})}(r_k,\ldots,r_k), \tag{54}$$

by replacing all $r_k^{(n)}$ in (53) with r_k, we get (22).

Appendix D
Proof of Theorem 4

For convenience, denote $\bar{\boldsymbol{a}}_{j,k}^n=(\bar{a}_{j,k}^{n,1},\ldots,\bar{a}_{j,k}^{n,M})^T$ and $\bar{\boldsymbol{b}}_{j,k}^n=(\bar{b}_{j,k}^{n,1},\ldots,\bar{b}_{j,k}^{n,M})^T$. According to the definition of $\overline{\Psi}_k$

$$\begin{aligned}&F_{(\Phi_k^{(1)},\ldots,\Phi_k^{(N)})}(r_k^{(1)},\ldots,r_k^{(N)})=\mathbb{E}_{(\boldsymbol{a}_{k,k},\boldsymbol{a}_{\bar{k},k},\boldsymbol{b}_{k,k},\boldsymbol{b}_{\bar{k},k})}\left[\prod_{n=1}^{N}F_{\Phi_k^{(n)}|(\boldsymbol{a}_{k,k},\boldsymbol{a}_{\bar{k},k},\boldsymbol{b}_{k,k},\boldsymbol{b}_{\bar{k},k})}(r_k^{(n)})\right]\\ &=\frac{1}{\pi^{2M}}\int_{-\infty}^{+\infty}\cdots\int_{-\infty}^{+\infty}\exp\left\{-\sum_{m=1}^{M}\left[\left(a_{k,k}^{(m)}\right)^2+\left(a_{\bar{k},k}^{(m)}\right)^2+\left(b_{k,k}^{(m)}\right)^2+\left(b_{\bar{k},k}^{(m)}\right)^2\right]\right\}\\ &\times\prod_{n=1}^{N}F_{\Phi_k^{(n)}|(\boldsymbol{a}_{k,k},\boldsymbol{a}_{\bar{k},k},\boldsymbol{b}_{k,k},\boldsymbol{b}_{\bar{k},k})}(r_k^{(n)})\;da_{k,k}^{(1)}\cdots da_{k,k}^{(M)}da_{\bar{k},k}^{(1)}\cdots da_{\bar{k},k}^{(M)}db_{k,k}^{(1)}\cdots db_{k,k}^{(M)}db_{\bar{k},k}^{(1)}\cdots db_{\bar{k},k}^{(M)}\end{aligned} \tag{53}$$

in (31), its CDF can be computed as

$$\begin{aligned}
&F_{\overline{\Psi}_k}(r_k)\\
&=\prod_{n=1}^{N}\Pr\left\{\overline{\Phi}_k^{n,l}\le r_k, 1\le l\le L\right\}\\
&=\prod_{n=1}^{N}\mathbb{E}_{(\bar{\boldsymbol{a}}_{k,k}^n,\bar{\boldsymbol{a}}_{\bar{k},k}^n,\bar{\boldsymbol{b}}_{k,k}^n,\bar{\boldsymbol{b}}_{\bar{k},k}^n)}\left[\Pr\left\{\overline{\Phi}_k^{n,l}\middle|(\bar{\boldsymbol{a}}_{k,k}^n,\bar{\boldsymbol{a}}_{\bar{k},k}^n,\bar{\boldsymbol{b}}_{k,k}^n,\bar{\boldsymbol{b}}_{\bar{k},k}^n)\right.\right.\\
&\qquad\left.\left.\le r_k, 1\le l\le L\right\}\right]\\
&\overset{(a)}{=}\prod_{n=1}^{N}\mathbb{E}_{(\bar{\boldsymbol{a}}_{k,k}^n,\bar{\boldsymbol{a}}_{\bar{k},k}^n,\bar{\boldsymbol{b}}_{k,k}^n,\bar{\boldsymbol{b}}_{\bar{k},k}^n)}\left[\prod_{l=1}^{L}\Pr\left\{\overline{\Phi}_k^{n,l}\middle|(\bar{\boldsymbol{a}}_{k,k}^n,\bar{\boldsymbol{a}}_{\bar{k},k}^n,\bar{\boldsymbol{b}}_{k,k}^n,\bar{\boldsymbol{b}}_{\bar{k},k}^n)\right.\right.\\
&\qquad\left.\left.\le r_k\right\}\right]\\
&\overset{(b)}{=}\prod_{n=1}^{N}\mathbb{E}_{(\bar{\boldsymbol{a}}_{k,k}^n,\bar{\boldsymbol{a}}_{\bar{k},k}^n,\bar{\boldsymbol{b}}_{k,k}^n,\bar{\boldsymbol{b}}_{\bar{k},k}^n)}\left[\left(F_{\overline{\Phi}_k^{n,l}|(\bar{\boldsymbol{a}}_{k,k}^n,\bar{\boldsymbol{a}}_{\bar{k},k}^n,\bar{\boldsymbol{b}}_{k,k}^n,\bar{\boldsymbol{b}}_{\bar{k},k}^n)}(r_k)\right)^L\right],
\end{aligned}\tag{55}$$

where (a) and (b) follow from the fact that given $(\bar{\boldsymbol{a}}_{k,k}^n,\bar{\boldsymbol{a}}_{\bar{k},k}^n,\bar{\boldsymbol{b}}_{k,k}^n,\bar{\boldsymbol{b}}_{\bar{k},k}^n)$, $\overline{\Phi}_k^{n,l}, 1\le l\le L$ are i.i.d. For a given $(\bar{\boldsymbol{a}}_{j,k}^n,\bar{\boldsymbol{b}}_{j,k}^n)$, $\overline{g}_{j,k}^{n,l}$ in (26) is Gaussian, i.e.,

$$\overline{g}_{j,k|(\bar{\boldsymbol{a}}_{j,k}^n,\bar{\boldsymbol{b}}_{j,k}^n)}^{n,l}\sim\mathcal{CN}\left(\sigma_{j,k}\sum_{m=1}^{M}\sqrt{\theta_m}u_{n,m}\left(\bar{a}_{j,k}^{n,m}+i\bar{b}_{j,k}^{n,m}\right),\right.$$
$$\left.\sigma_{j,k}^2\left(1-\sum_{m=1}^{M}\theta_m u_{n,m}^2\right)\right).\tag{56}$$

Hence, $\left|\overline{g}_{j,k|(\bar{\boldsymbol{a}}_{j,k}^n,\bar{\boldsymbol{b}}_{j,k}^n)}^{n,l}\right|$ is Rice or Rician distributed, i.e.,

$$\left|\overline{g}_{j,k|(\bar{\boldsymbol{a}}_{j,k}^n,\bar{\boldsymbol{b}}_{j,k}^n)}^{n,l}\right|\sim\text{Rice}\left(\sqrt{\overline{\alpha}_{j,k}^{(n)}},\sqrt{\overline{\beta}_{j,k}^{(n)}}\right),\tag{57}$$

where

$$\begin{cases}\overline{\alpha}_{j,k}^{(n)}=\sigma_{j,k}^2\left[\left(\sum_{m=1}^{M}\sqrt{\theta_m}u_{n,m}\bar{a}_{j,k}^{n,m}\right)^2+\left(\sum_{m=1}^{M}\sqrt{\theta_m}u_{n,m}\bar{b}_{j,k}^{n,m}\right)^2\right],\\ \overline{\beta}_{j,k}^{(n)}=\dfrac{\sigma_{j,k}^2}{2}\left(1-\sum_{m=1}^{M}\theta_m u_{n,m}^2\right).\end{cases}\tag{58}$$

Then, given $(\bar{\boldsymbol{a}}_{k,k}^n,\bar{\boldsymbol{a}}_{\bar{k},k}^n,\bar{\boldsymbol{b}}_{k,k}^n,\bar{\boldsymbol{b}}_{\bar{k},k}^n)$, the CDF of $\overline{\Phi}_k^{n,l}$ is given by

$$\begin{aligned}
&F_{\overline{\Phi}_k^{n,l}|(\bar{\boldsymbol{a}}_{k,k}^n,\bar{\boldsymbol{a}}_{\bar{k},k}^n,\bar{\boldsymbol{b}}_{k,k}^n,\bar{\boldsymbol{b}}_{\bar{k},k}^n)}(r_k)\\
&=1-\int_0^{+\infty}Q_1\left(\sqrt{\frac{\overline{\alpha}_{k,k}^{(n)}}{\overline{\beta}_{k,k}^{(n)}}},\frac{r_k z}{\sqrt{\overline{\beta}_{k,k}^{(n)}}}\right)\frac{z}{\overline{\beta}_{\bar{k},k}^{(n)}}\exp\left(-\frac{z^2+\overline{\alpha}_{\bar{k},k}^{(n)}}{2\overline{\beta}_{\bar{k},k}^{(n)}}\right)\\
&\qquad\times I_0\left(\frac{\sqrt{\overline{\alpha}_{\bar{k},k}^{(n)}}}{\overline{\beta}_{\bar{k},k}^{(n)}}z\right)dz.
\end{aligned}\tag{59}$$

It can be observed from (58) that $\overline{\alpha}_{j,k}^{(n)}$ is a sum square of Gaussian variables, and thus follows Chi-squared distribution. According to [32, (68)], the PDF of $\overline{\alpha}_{j,k}^{(n)}$ is given by

$$f_{\overline{\alpha}_{j,k}^{(n)}}(\alpha)=\frac{1}{\sigma_{j,k}^2\xi_n}\exp\left(-\frac{\alpha}{\sigma_{j,k}^2\xi_n}\right),\ \forall\ \alpha\ge 0,\tag{60}$$

where $\xi_n=\sum_{m=1}^{M}\theta_m u_{n,m}^2$. Then, based on (59) and (60), we have

$$\begin{aligned}
&\mathbb{E}_{(\bar{\boldsymbol{a}}_{k,k}^n,\bar{\boldsymbol{a}}_{\bar{k},k}^n,\bar{\boldsymbol{b}}_{k,k}^n,\bar{\boldsymbol{b}}_{\bar{k},k}^n)}\left[F_{\overline{\Phi}_k^{n,l}|(\bar{\boldsymbol{a}}_{k,k}^n,\bar{\boldsymbol{a}}_{\bar{k},k}^n,\bar{\boldsymbol{b}}_{k,k}^n,\bar{\boldsymbol{b}}_{\bar{k},k}^n)}(r_k)\right]^L\\
&=\mathbb{E}_{(\overline{\alpha}_{k,k}^{(n)},\overline{\alpha}_{\bar{k},k}^{(n)})}\left[1-\int_0^{+\infty}Q_1\left(\sqrt{\frac{\overline{\alpha}_{k,k}^{(n)}}{\overline{\beta}_{k,k}^{(n)}}},\frac{r_k z}{\sqrt{\overline{\beta}_{k,k}^{(n)}}}\right)\frac{z}{\overline{\beta}_{\bar{k},k}^{(n)}}\right.\\
&\left.\times\exp\left(-\frac{z^2+\overline{\alpha}_{\bar{k},k}^{(n)}}{2\overline{\beta}_{\bar{k},k}^{(n)}}\right)I_0\left(\frac{\sqrt{\overline{\alpha}_{\bar{k},k}^{(n)}}}{\overline{\beta}_{\bar{k},k}^{(n)}}z\right)dz\right]^L\\
&=\frac{1}{\sigma_{k,k}^2\sigma_{\bar{k},k}^2\xi_n^2}\int_0^{+\infty}\int_0^{+\infty}\exp\left(-\frac{\alpha_1}{\sigma_{k,k}^2\xi_n}-\frac{\alpha_2}{\sigma_{\bar{k},k}^2\xi_n}\right)\\
&\times\left[1-\int_0^{+\infty}Q_1\left(\sqrt{\frac{\alpha_1}{\overline{\beta}_{k,k}^{(n)}}},\frac{r_k z}{\sqrt{\overline{\beta}_{k,k}^{(n)}}}\right)\frac{z}{\overline{\beta}_{\bar{k},k}^{(n)}}\exp\left(-\frac{z^2+\alpha_2}{2\overline{\beta}_{\bar{k},k}^{(n)}}\right)\right.\\
&\left.\times I_0\left(\frac{\sqrt{\alpha_2}}{\overline{\beta}_{\bar{k},k}^{(n)}}z\right)dz\right]^L d\alpha_1 d\alpha_2.
\end{aligned}\tag{61}$$

Substituting (61) into (55), we obtain (33).

Appendix E
Proof of Theorem 5

If M is large enough such that $\xi_n\to 1$, then we have $1-\sum_{m=1}^{M}\theta_m u_{n,m}^2\approx 0$. Hence, the second term of (26) can be ignored, i.e.,

$$\overline{g}_{j,k}^{n,l}\approx\sigma_{j,k}\sum_{m=1}^{M}\sqrt{\theta_m}u_{n,m}\left(\bar{a}_{j,k}^{n,m}+i\bar{b}_{j,k}^{n,m}\right)\triangleq\check{g}_{j,k}^{n,l}.\tag{62}$$

It is obvious that

$$|\check{g}_{j,k}^{n,l}|=\sqrt{\overline{\alpha}_{j,k}^{(n)}},\tag{63}$$

in which $\overline{\alpha}_{j,k}^{(n)}$ is given in (58). Based on the PDF of $\overline{\alpha}_{j,k}^{(n)}$ provided in (60), we could obtain its CDF as

$$\begin{aligned}
F_{\overline{\alpha}_{j,k}^{(n)}}(\alpha)&=\int_0^{+\infty}\frac{1}{\sigma_{j,k}^2\xi_n}\exp\left(-\frac{z}{\sigma_{j,k}^2\xi_n}\right)dz\\
&=1-\exp\left(-\frac{\alpha}{\sigma_{j,k}^2\xi_n}\right),\ \forall\alpha\ge 0.
\end{aligned}\tag{64}$$

Denote

$$\begin{cases}\check{\Phi}_k^{n,l}=\dfrac{|\check{g}_{k,k}^{n,l}|}{|\check{g}_{\bar{k},k}^{n,l}|},\\ \check{\Psi}_k=\max\left\{\check{\Phi}_k^{n,l},1\le n\le N,1\le l\le L\right\}.\end{cases}\tag{65}$$

It is known from (62) that for a given n,

$$\check{\Phi}_k^{n,l_1}=\check{\Phi}_k^{n,l_2},\ \forall\ 1\le l_1,l_2\le L,\tag{66}$$

indicating that the columns of the $N \times L$ dimensional matrix consisting of $\check{\Phi}_k^{n,l}, 1 \le n \le N, 1 \le l \le L$ are all the same. In addition, since $\overline{g}_{j,k}^{n,l} \approx \check{g}_{j,k}^{n,l}$, we have

$$\begin{cases} \overline{\Phi}_k^{n,l} \approx \check{\Phi}_k^{n,l}, \ \forall\ 1 \le n \le N, \ 1 \le l \le L, \ 1 \le k \le K, \\ \overline{\Psi}_k \approx \check{\Psi}_k, \ \forall\ 1 \le k \le K, \end{cases} \tag{67}$$

where $\overline{\Phi}_k^{n,l}$ and $\overline{\Psi}_k$ are defined in (31). Now we compute the CDF of $\check{\Psi}_k$. First, we have the CDF of $\check{\Phi}_k^{n,l}$ given by

$$\begin{aligned} &F_{\check{\Phi}_k^{n,l}}(r_k) \\ &= \Pr\left\{\check{g}_{k,k}^{n,l} \le \check{g}_{\bar{k},k}^{n,l} r_k\right\} = \Pr\left\{\overline{\alpha}_{k,k}^{(n)} \le \overline{\alpha}_{\bar{k},k}^{(n)} r_k^2\right\} \\ &= \int_0^{+\infty} F_{\overline{\alpha}_{k,k}^{(n)}}(\alpha r_k^2) f_{\overline{\alpha}_{\bar{k},k}^{(n)}}(\alpha) d\alpha \\ &= \int_0^{+\infty} \left[1 - \exp\left(-\frac{\alpha r_k^2}{\sigma_{k,k}^2 \xi_n}\right)\right] \frac{1}{\sigma_{\bar{k},k}^2 \xi_n} \exp\left(-\frac{\alpha}{\sigma_{\bar{k},k}^2 \xi_n}\right) d\alpha \\ &= \frac{r_k^2}{1 + r_k^2}, \end{aligned} \tag{68}$$

where the last step holds due to the assumption that $\sigma_{k,k} = \sigma_{\bar{k},k}$. Then, we can derive that

$$\begin{aligned} F_{\check{\Psi}_k}(r_k) &= \Pr\left\{\check{\Phi}_k^{n,l} \le r_k, 1 \le n \le N, 1 \le l \le L\right\} \\ &\overset{(a)}{=} \Pr\left\{\check{\Phi}_k^{n,l} \le r_k, 1 \le n \le N\right\} \\ &\overset{(b)}{=} \prod_{n=1}^{N} \Pr\left\{\check{\Phi}_k^{n,l} \le r_k\right\} \\ &\overset{(c)}{=} \left(\frac{r_k^2}{1 + r_k^2}\right)^N, \end{aligned} \tag{69}$$

where (a) holds due to (66), (b) follows from the fact that for a given l, $\check{\Phi}_k^{n,l}, \forall 1 \le n \le N$ are independent, and (c) is obtained by using (68). Combining (67) and (69), Theorem 5 can be proven.

REFERENCES

[1] F. Tariq *et al.*, "A speculative study on 6G," *IEEE Wireless Commun.*, vol. 27, no. 4, pp. 118–125, Aug. 2020.

[2] E. G. Larsson, O. Edfors, F. Tufvesson, and T. L. Marzetta, "Massive MIMO for next generation wireless systems," *IEEE Commun. Mag.*, vol. 52, no. 2, pp. 186–195, Feb. 2014.

[3] Z. Wang *et al.*, "Extremely large-scale MIMO: Fundamentals, challenges, solutions, and future directions," *IEEE Wireless Commun.*, Apr. 2023.

[4] Y. Saito *et al.*, "Non-orthogonal multiple access (NOMA) for cellular future radio access," in *Proc. IEEE Veh. Technol. Conf. Spring (VTC-Spring)*, 2-5 Jun. 2013, Dresden, Germany.

[5] L. Dai *et al.*, "Non-orthogonal multiple access for 5G: solutions, challenges, opportunities, and future research trends," *IEEE Commun. Mag.*, vol. 53, no. 9, pp. 74–81, Sep. 2015.

[6] N. Ye, J. An, *et al.*, "Deep-learning-enhanced NOMA transceiver design for massive MTC: Challenges, state of the art, and future directions," *IEEE Wireless Commun.*, vol. 28, no. 4, pp. 66–73, Aug. 2021.

[7] Y. Mao *et al.*, "Rate-splitting multiple access: Fundamentals, survey, and future research trends," *IEEE Commun. Surv. & Tut.*, vol. 24, no. 4, pp. 2073–2126, 2022.

[8] K.-K. Wong, K.-F. Tong, Y. Zhang, and Z. Zhongbin, "Fluid antenna system for 6G: When Bruce Lee inspires wireless communications," *Elect. Lett.*, vol. 56, no. 24, pp. 1288–1290, Nov. 2020.

[9] A. Shojaeifard *et al.*, "MIMO evolution beyond 5G through reconfigurable intelligent surfaces and fluid antenna systems," *Proc. IEEE*, vol. 110, no. 9, pp. 1244–1265, Sep. 2022.

[10] Y. Huang, L. Xing, C. Song, S. Wang, and F. Elhouni, "Liquid antennas: Past, present and future," *IEEE Open J. Antennas & Prop.*, vol. 2, pp. 473–487, Mar. 2021.

[11] A. Dey, R. Guldiken, and G. Mumcu, "Microfluidically reconfigured wideband frequency-tunable liquid-metal monopole antenna," *IEEE Trans. Antennas & Propag.*, vol. 64, no. 6, pp. 2572–2576, Jun. 2016.

[12] K. N. Paracha, A. D. Butt, A. S. Alghamdi, S. A. Babale, and P. J. Soh, "Liquid metal antennas: Materials, fabrication and applications," *Sensors*, vol. 20, no. 1, p. 177, Dec. 2019.

[13] D. Rodrigo, B. A. Cetiner and L. Jofre, "Frequency, radiation pattern and polarization reconfigurable antenna using a parasitic pixel layer," *IEEE Trans. Antennas & Propag.*, vol. 62, no. 6, pp. 3422–3427, Jun. 2014.

[14] S. Song and R. D. Murch, "An efficient approach for optimizing frequency reconfigurable pixel antennas using genetic algorithms," *IEEE Trans. Antennas & Propag.*, vol. 62, no. 2, pp. 609–620, Feb. 2014.

[15] T. V. Hoang, V. Fusco, *et al.*, "Computational polarimetric imaging using two-dimensional dynamic metasurface apertures," *IEEE Open J. Antennas & Propag.*, vol. 2, pp. 488–497, Mar. 2021.

[16] T. Ismail and M. M. Dawoud, "Null steering in phased arrays by controlling the element positions," *IEEE Trans. Antennas & Prop.*, vol. 39, no. 11, pp. 1561–1566, Nov. 1991.

[17] S. Basbug, "Design and synthesis of antenna array with movable elements along semicircular paths," *IEEE Antennas Wireless Prop. Lett.*, vol. 16, pp. 3059–3062, Oct. 2017.

[18] M. C. Johnson, S. L. Brunton, N. B. Kundtz, and J. N. Kutz, "Sidelobe canceling for reconfigurable holographic metamaterial antenna," *IEEE Trans. Antennas & Prop.*, vol. 63, no. 4, pp. 1881–1886, Apr. 2015.

[19] K.-K. Wong, A. Shojaeifard, K.-F. Tong, and Y. Zhang, "Fluid antenna systems," *IEEE Trans. Wireless Commun.*, vol. 20, no. 3, pp. 1950–1962, Mar. 2021.

[20] P. Mukherjee, C. Psomas, and I. Krikidis, "On the level crossing rate of fluid antenna systems," in *Proc. IEEE 23rd Int. Workshop Sig. Process. Advances Wireless Commun. (SPAWC)*, 4-6 Jul. 2022, Oulu, Finland.

[21] L. Tlebaldiyeva, G. Nauryzbayev, S. Arzykulov, A. Eltawil, and T. Tsiftsis, "Enhancing QoS through fluid antenna systems over correlated nakagami-m fading channels," in *Proc. IEEE Wireless Commun. Netw. Conf. (WCNC)*, 10-13 Apr. 2022, Austin, TX, USA.

[22] L. Tlebaldiyeva, S. Arzykulov, K. M. Rabie, X. Li, and G. Nauryzbayev, "Outage performance of fluid antenna system (FAS)-aided Terahertz communication networks," in *Proc. IEEE Int. Conf. Commun. (ICC)*, 28 May-1 Jun. 2023, Rome, Italy.

[23] C. Psomas, G. M. Kraidy, K.-K. Wong, and I. Krikidis, "On the diversity and coded modulation design of fluid antenna systems," [Online] arXiv preprint arXiv:2205.01962, 2022.

[24] B. Tang, H. Xu, K.-K. Wong, K. Tong, Y. Zhang, and C. B. Chae, "Fluid Antenna Enabling Secret Communications," *IEEE Commun. Lett.*, vol. 27, no. 6, pp. 1941–1945, Jun. 2023.

[25] W. K. New, K.-K. Wong, H. Xu, K. Tong, and C. B. Chae, "Fluid antenna system: New insights on outage probability and diversity gain," *IEEE Trans. Wireless Commun.*, vol. 23, no. 1, pp. 128–140, Jan. 2024.

[26] K.-K. Wong and K.-F. Tong, "Fluid antenna multiple access," *IEEE Trans. Wireless Commun.*, vol. 21, no. 7, pp. 1950–1962, Jul. 2022.

[27] K. Wong, K. Tong, Y. Chen, and Y. Zhang, "Closed-form expressions for spatial correlation parameters for performance analysis of fluid antenna systems," *IET Elect. Lett.*, vol. 58, no. 11, pp. 454–457, May 2022.

[28] K. K. Wong, D. Morales-Jimenez, K. F. Tong, and C. B. Chae, "Slow fluid antenna multiple access," *IEEE Trans. Commun.*, vol. 71, no. 5, pp. 2831–2846, May 2023.

[29] C. Skouroumounis, I. Krikidis, "Fluid antenna with linear MMSE channel estimation for large-scale cellular networks," *IEEE Trans. Commun.*, vol. 71, no. 2, pp.1112-1125, Feb. 2023.

[30] L. Tlebaldiyeva, S. Arzykulov, T. A. Tsiftsis, and G.Nauryzbayev, "Full-duplex cooperative NOMA-based mmWave networks with fluid antenna system (FAS) receivers," in *Proc. Int. Balkan Conf. Commun. Networking (BalkanCom)*, Istanbul, Turkiye, Jun. 2023, pp. 1-6.

[31] N. C. Beaulieu and K. T. Hemachandra, "Novel simple representations for Gaussian class multivariate distributions with generalized correlation," *IEEE Trans. Inf. Theory*, vol. 57, no. 12, pp. 8072–8083, Dec. 2011.

[32] M. Khammassi, A. Kammoun, and M.-S. Alouini, "A new analytical approximation of the fluid antenna system channel," *IEEE Trans. Wireless Commun.*, vol. 22, no. 12, pp. 8843–8858, Dec. 2023.

[33] H. Xu, K. K. Wong, W. K. New, and K. F. Tong, "On outage probability for two-user fluid antenna multiple access," in *Proc. IEEE Int. Conf. Commun. (ICC)*, 28 May-1 Jun. 2023, Rome, Italy.

[34] W. K. New, K.-K. Wong, X. Hao, K.-F. Tong, and C.-B. Chae, "An information-theoretic characterization of MIMO-FAS: Optimization, diversity-multiplexing tradeoff and q-outage capacity," *IEEE Trans. Wireless Commun.*, early access, DOI: 10.1109/TWC.2023.3327063.
[35] W. C. Jakes and D. C. Cox, *Microwave mobile communications*, Wiley-IEEE press, 1994.
[36] H. Xu, G. Zhou, K. K Wong, et al., "Channel estimation for FAS-assisted multiuser mmWave systems." *IEEE Commun. Lett.*, early access, DOI: 10.1109/LCOMM.2023.3347951.
[37] S. Serra, "On the extreme eigenvalues of Hermitian (block) Toeplitz matrices," *Linear Alg. Its Appl.*, vol. 270, no. 1-3, pp. 109–129, 1998.

Hao Xu (S'15 – M'19) received the B.S. degree in communication engineering from Nanjing University of Science and Technology, Nanjing, China, in 2013, and the Ph.D. degree in information and communication engineering with the National Mobile Communications Research Laboratory, Southeast University, Nanjing, China, in 2019. From 2019 to 2021, he was an Alexander von Humboldt (AvH) Post-Doctoral Research Fellow with the Faculty of Electrical Engineering and Computer Science at the Technical University of Berlin, Germany. He is currently a Marie Skłodowska-Curie Actions (MSCA) Individual Fellow with the Department of Electronic and Electrical Engineering, University College London, UK. His research interests mainly include information theory, mathematical optimization, MIMO systems, D2D communication, and physical layer security in wireless networks.

(Kit) Kai-Kit Wong (M'01-SM'08-F'16) received the BEng, the MPhil, and the PhD degrees, all in Electrical and Electronic Engineering, from the Hong Kong University of Science and Technology, Hong Kong, in 1996, 1998, and 2001, respectively. After graduation, he took up academic and research positions at the University of Hong Kong, Lucent Technologies, Bell-Labs, Holmdel, the Smart Antennas Research Group of Stanford University, and the University of Hull, UK. He is Chair in Wireless Communications at the Department of Electronic and Electrical Engineering, University College London, UK.

His current research centers around 5G and beyond mobile communications. He is a co-recipient of the 2013 IEEE Signal Processing Letters Best Paper Award and the 2000 IEEE VTS Japan Chapter Award at the IEEE Vehicular Technology Conference in Japan in 2000, and a few other international best paper awards. He is Fellow of IEEE and IET and is also on the editorial board of several international journals. He served as the Editor-in-Chief for IEEE Wireless Communications Letters between 2020 and 2023.

(Aven) Wee Kiat New received his Ph.D in Electrical Engineering from Universiti Teknologi Malaysia, M.Eng.Sc in Electrical Engineering from University of Malaya and B.IT in Data Communications and Networking from Multimedia University. He was a visiting researcher at Lancaster University and University of Cyprus. He is currently a research fellow at the Department of Electronic and Electrical Engineering, University College London, UK. His research interests are information theory, optimization, stochastic processes, machine learning and their applications in emerging areas of communications. He was the recipient of the 2021 IEEE Malaysia Comsoc/VTS best paper award, 2021 and 2020 IEEE Malaysia AP/MTT/EMC best paper awards.

(Kenneth) Kin-Fai Tong (M'99-SM'13-F'23) received the B.Eng. and Ph.D. degrees in electronic engineering from the City University of Hong Kong in 1993 and 1997, respectively. After graduation, Dr. Tong worked in the Department of Electronic Engineering at City University of Hong Kong as a Research Fellow. Two years later, he took up the post Expert researcher in the Photonic Information Technology Group and Millimetre-wave Devices Group at the National Institute of Information and Communications Technology (NiCT), Japan, where his main research focused on photonic-millimeter-wave planar antennas at 10GHz, 38 GHz and 60 GHz for high-speed wireless communications systems. In 2005, he started his academic career in the Department of Electronic and Electrical Engineering, UCL, as a lecturer. Now Dr. Tong is Chair in Antennas in the department. His current research interests include millimeter-wave and THz antennas, fluid antennas, 3D printed antennas and sub-GHz long range IoT networks. He served as the General Co-Chair of the 2017 International Workshop on Electromagnetics (iWEM), and Lead Guest Editor of IEEE OJAP in 2020.

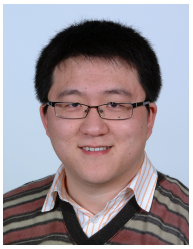

Yangyang Zhang received the B.S. and M.S. degrees in electronics and information engineering from Northeastern University, Shenyang, China, in 2002 and 2004 respectively, and the Ph.D. degree in electrical engineering from the University of Oxford, Oxford, U.K., in 2008. He is currently taking the position of Executive Director of Kuang-Chi Science Limited, Hong Kong. His research interests include multiple-input multiple-output wireless communications and stochastic optimization algorithms. Dr. Zhang has been awarded more than 20 honors. Besides, he also authored and co-authored more than 40 refereed papers.

Chan-Byoung Chae (S'06-M'09-SM'12-F'21) is an Underwood Distinguished Professor in the School of Integrated Technology, Yonsei University, Korea. Before joining Yonsei University, he was with Bell Labs, Alcatel-Lucent, Murray Hill, NJ, USA from 2009 to 2011, as a Member of Technical Staff, and Harvard University, Cambridge, MA, USA from 2008 to 2009, as a Postdoctoral Research Fellow. He received his Ph.D. degree in Electrical & Computer Engineering from The University of Texas at Austin in 2008. Prior to joining UT, he was a research engineer at the Telecommunications R&D Center, Samsung Electronics, Suwon, Korea, from 2001 to 2005.

He has been an Editor-in-Chief of the IEEE Trans. Molecular, Biological, and Multi-scale Communications (2019-2022) and a Senior Editor of the IEEE Wireless Communications Letters (2020-present). He has served/serves as an Editor for the IEEE Communications Magazine (2016-present), the IEEE Trans. on Wireless Communications (2012-2017), and the IEEE Wireless Communications Letters (2016-present). He is an IEEE ComSoc Distinguished Lecturer for the term 2020-2021 and 2022-2023.

He was the recipient/co-recipient of the CES Innovation Award in 2023, the IEEE ICC Best Demo Award in 2022, the IEEE WCNC Best Demo Award in 2020, the Best Young Engineer Award from the National Academy of Engineering of Korea (NAEK) in 2019, the IEEE DySPAN Best Demo Award in 2018, the IEEE/KICS Journal of Communications and Networks Best Paper Award in 2018, the IEEE INFOCOM Best Demo Award in 2015, the IEIE/IEEE Joint Award for Young IT Engineer of the Year in 2014, the KICS Haedong Young Scholar Award in 2013, the IEEE Signal Processing Magazine Best Paper Award in 2013, the IEEE ComSoc AP Outstanding Young Researcher Award in 2012, the IEEE VTS Dan. E. Noble Fellowship Award in 2008.